applied to SDS-17.5% polyacrylamide gels under reducing conditions and transferred onto a polyvinylidene fluoride membrane (Millipore, Bedford, Mass., U.S.A.). After blocking non-specific protein binding using Tris-buffered saline-Tween 20 (TBST) containing 5% fat-free dry milk, the membrane was incubated with rabbit anti-S100A4 pAb for 1 hr at room temperature, followed by reaction with secondary antibody conjugated with peroxidase. After washing with TBST three times, signals were detected by chemiluminescence with an ECL kit (Amersham Pharmacia Biotech).

FACS analysis of cell surface antigen. RNK16 cells were washed twice with PBS and harvested by 5 mM PBS-EDTA. They were incubated with #067 mAb supernatant, rabbit anti-S100A4 pAb for 30 min at 4 C. After washing twice with PBS, cells were incubated with 50 μl of FITC-conjugated goat anti-mouse IgG (Kirkegaard & Perry Laboratories, Gaithersburg, Md., U.S.A.) for 30 min at 4 C. Cells were fixed in 1% paraformaldehyde-PBS and subjected to a FACS analyzer (BD Bioscience). Parallel samples for control were stained with isotype-matched mAb or PBS.

Reactivity of TCRγδ T cell hybridomas. Established hybridoma clones were stained with anti-CD3, -CD4, -CD8, -TCRγδ, and -NKR-P1 followed by goat anti-mouse IgG+IgM second antibody conjugated with FITC. They were analyzed by fluorescence activated cell sorting (FACS) for the identification of their profile. Hybridoma cells (1×10^5/well) seeded in a 96-microwell plate were tested for their reactivity with 0.5×10^5/well RNK16 cells. The supernatants of hybridomas co-cultured with target cells for 12–18 hr were transferred and tested for TNF production. In the blocking assay, target cells were pretreated with either #067 mAb or rabbit anti-S100A4 pAb. TNF concentration was measured by a Wehi 164 cell mortality assay or directly measured by ELISA (Biosource International, Camarillo, Calif., U.S.A.). All experiments were conducted in triplicate and repeated three times.

Results

Expression Cloning of #067 Antigen

We first constructed the W31 cDNA library as described in "Materials and Methods." We initially obtained about 8×10^5 independent clones on the agarose plates. To confirm the quality of the library, we selected 10 clones at random and digested them with *Eco*RI to examine the insert length. Based on the results from gel electrophoresis, we estimated that the incorporation efficiency was 90%; the insert range was 400–2,700 bp and the average length of the insert cDNA was 1,163 bp (Fig. 1).

Consequently, we performed expression cloning of the #067 antigen as described in "Materials and Methods." After immunoscreening about 150,000 clones with #067 mAb, No. 293-2-10 was sounded to show reactivity for the antibody (Fig. 2). Nucleotide sequence of No. 293-2-10 was completely matched with that of rat S100A4 cDNA. To further confirm the reactivity of #067 mAb with S100A4, we transiently transfected HEK293 cells with the full length form of the S100A4 gene and examined them by immunocytochemistry. In accordance with the result from No. 293-2-10, these cells exhibited the same reactivity against #067 mAb with S100A4 protein as they did with #067 mAb (Fig. 3).

The Higher Expression of S100A4 in W31 Cells

We previously reported that #067 antigen was up-regulated on W31 cells which were transformed by H-

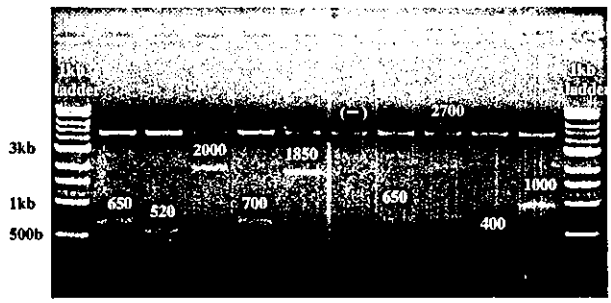

Fig. 1. Quality of cDNA library from the W31 cell line. After 10 clones were selected at random from the initial W31 cDNA library, each plasmid was digested with *Eco*RI and *Xho*I and the insert lengths were examined by gel electrophoresis.

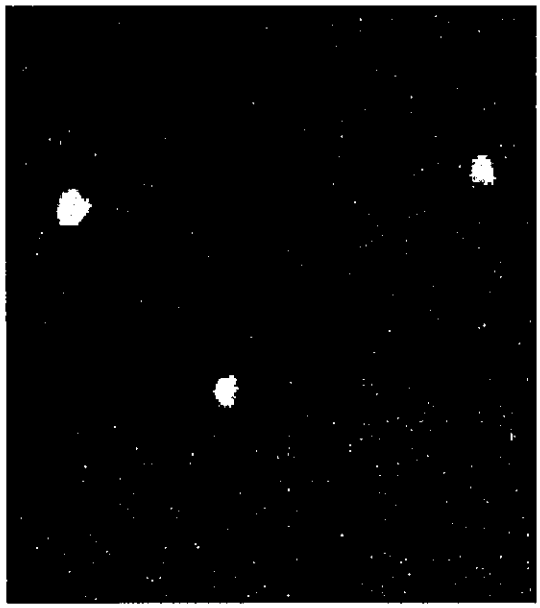

Fig. 2. Final stage for immunostaining screening of HEK293 transiently transfected with No. 293-2-10 (single clone) stained with #067 mAb. Original magnification: ×600.

ras oncogene. Accordingly, to confirm this fact, we first assessed the transcripts of S100A4 using northern blot analysis on both W31 and WFB cells. As was expected, the transcripts of S100A4 were up-regulated in W31 more than in WFB (Fig. 4). Next, we examined the expression of S100A4 protein using western blot analysis. The expression of S100A4 protein was clearly up-regulated in W31 cells, whereas the expression of S100A4 protein was only faintly detected in WFB cells at protein level (Fig. 5).

#067 Antigen and S100A4 Expression in W31 Cells

In our previous study, #067 antigen was found to be expressed on the cell surface of W31 cells (19). Therefore, S100A4, as well as #067 antigen, should be evident on the cell surface. To confirm whether S100A4 was expressed on the cell surface, we performed FACS analysis as described in "Materials and Methods." As predicted, S100A4 was obviously expressed on the cell surface (Fig. 6). To further determine whether both #067 antigen and S100A4 showed the same localization in W31 cells, we carried out double staining of W31 with #067 mAb and anti-S100A4 pAb. The localization

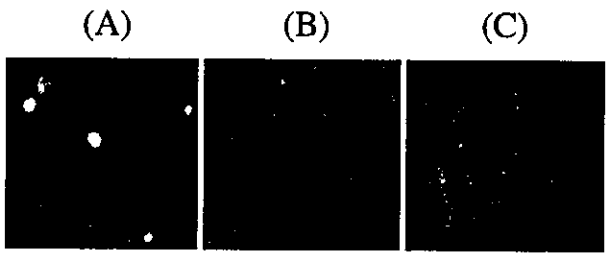

Fig. 3. Immunostaining analysis of HEK293 transfectants with #067 mAb. (A) Cells transiently transfected with pcDNA3.1-full length S100A4 cDNA were positive for #067 mAb. (B) Cells transfected with pcDNA3.1-full length S100A4 cDNA were negative for control antibody. (C) Cells transfected with mock pcDNA3.1 vector were negative for #067 mAb. Original magnification: ×600.

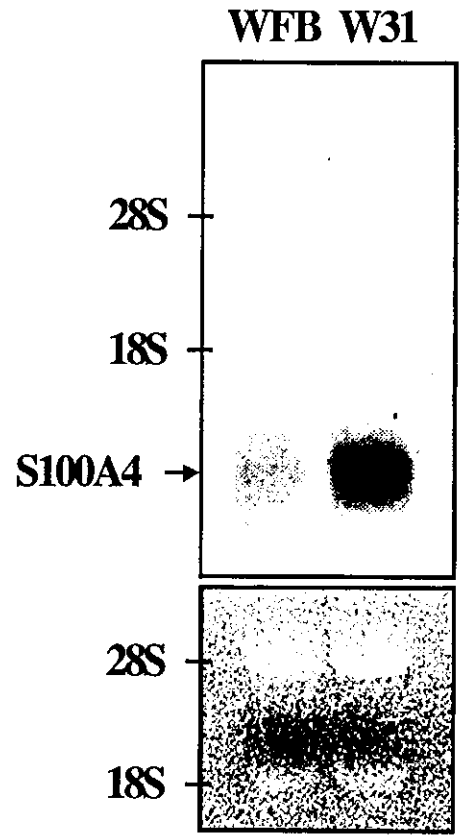

Fig. 4. Northern blot analysis of the S100A4 transcript in WFB and W31 cell lines. The presence of S100A4 transcript was analyzed using rat S100A4 cDNA obtained from RT-PCR product of W31 cells. The distribution of the transcript in 10 μg of poly(A)+ RNA from both cell lines indicated high levels of S100A4 transcript of approximately 0.5 kb in length in both cell lines. Note the higher levels in W31 than in WFB. Ethidium bromide staining of the gel is also shown.

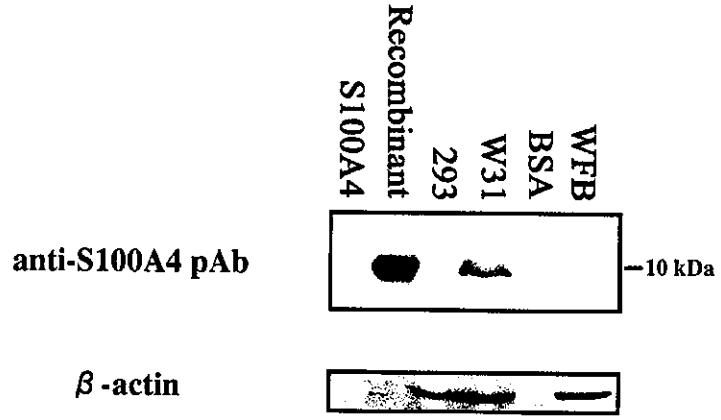

Fig. 5. Western blot analysis of S100A4 protein. Whole cell lysate of WFB and W31 were separated by SDS-PAGE and transferred to blotting membrane. Transferred proteins were immunoblotted with S100A4 pAb. The band of S100A4 protein detected in W31 was stronger than that in WFB. Recombinant S100A4 protein was a positive control, BSA and cell lysate of HEK293 cells were negative controls. Separate immunoblotting was performed with an anti-β actin mAb as a control.

of #067 antigen and S100A4 looked to be mainly in cytoplasm as well as on the cell surface. These results indicated that these two antibodies partially showed the same distribution in W31 cells (Fig. 7).

S100A4, a Possible Target Molecule of TCRγδ T Cell Hybridomas

In our previous study, we established #067-restricted and #067-non-restricted TCRγδ T cell hybridomas. We also reported that, using these hybridomas, #067 antigen reacted with #067-restricted FT126.1 cells of TCRγδ T cell hybridomas in an MHC-unrestricted manner. In this study, we attempted to determine whether S100A4 had similar properties to the #067 antigen. To do so we used #067 antigen expressing rat NK lymphoma cells (i.e.: RNK16 cells) as the target cells and used a TNF production assay to examine the reactivity of FT126.1 cells with S100A4 (15, 17). FT126.1 reacted against immobilized mAb V65 (mouse anti-rat TCRγδ mole-

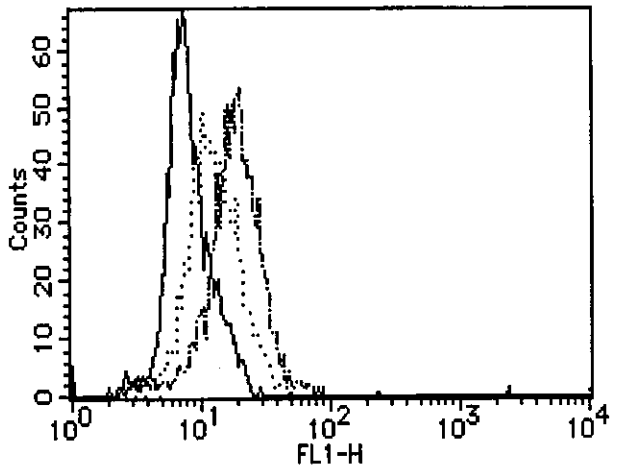

Fig. 6. Histograms obtained by flow cytometric analysis of RNK16 cell lines using #067 mAb (dotted line) and S100A4 pAb (dashed line). In control experiments, cells stained with mouse IgG were used (solid line). *X*-axis: fluorescence intensity in arbitrary units. *Y*-axis: number of cells.

#067 mAb **S100A4 pAb** **merge**

Fig. 7. Confocal laser microscopy after double staining with #067 mAb and S100A4 pAb. Original magnification: ×600.

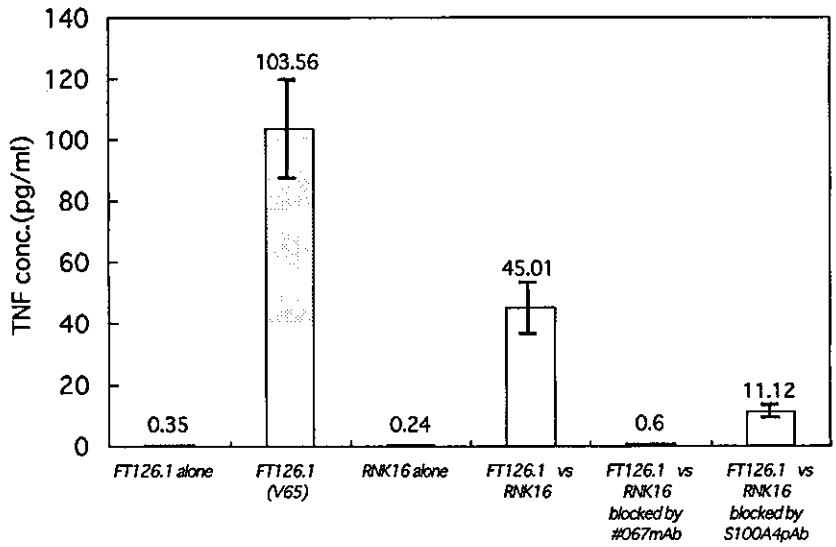

Fig. 8. Reactivities of TCRγδ T cell hybridoma (FT126.1) and blocking effects of #067 mAb and S100A4 pAb against the reactivities of TCRγδ T cell hybridoma (FT126.1) to RNK16. 1×10^5 cells/well of FT126.1 were incubated with immobilized mAb V65 and 0.5×10^5 cells/well of RNK16 in a 96-well microplate for 12–18 hr and the supernatant was measured for released TNF by ELISA. RNK16 cells were pretreated with #067 mAb and S100A4 pAb, respectively. Thereafter they were co-cultured with TCRγδ T cell hybridoma (FT126.1). Columns indicate mean value of triplicates. Bars indicate ±SE.

cules) and RNK16, showing high production of TNF. While strong reactivity inhibition was observed, the percentage inhibition obtained with #067 mAb and rabbit anti-S100A4 pAb was 98.7% and 75.3% respectively (Fig. 8). Thus, while the percentage of inhibition did vary, these results suggest that #067 and S100A4 might have functionally similar capacity against TCRγδ molecules of FT126.1.

Discussion

In our previous studies, it was shown that WKA rat splenic DNT cell lines were cytotoxic against syngeneic W31 as well as RNK16 cells in #067-restricted manner (29, 33). Since the interaction between CD4(−), CD8(−) DNT cells and the #067 molecule was inhibited by V65 mAb which reacts with a non-polymorphic determinant of rat TCRγδ molecules, we also suggested that #067 molecules were involved in TCRγδ T cell-mediated cytotoxicity (17). Moreover, we established #067-restricted TCRγδ T cell hybridomas and determined the TCRγδ usage and diversity in the genetic structure (15, 17).

In our present study, to determine the protein sequence of the #067 molecule, we carried out cDNA expression cloning of this molecule and found a protein that behaved in a very similar manner. After expression as well as functional analysis, we determined that the rat protein, S100A4, was a possible match for the #067 antigen.

S100A4 belongs to the S100 protein family, which consists of 19 small, acidic, calcium-binding proteins with two common EF-hand structural motifs (7, 12). S100A4 has been linked to the invasive and metastatic phenotype of cancer cells by evidence derived from transfections with expression constructs (4, 8, 22, 26, 31), from studies of transgenic animals (1, 5), as well as from clinical data (16, 24, 27, 34). S100A4 has initially been identified as a cytoplasmic protein that co-localizes or co-sediments with many different proteins including cytoskeletal molecules such as actin, non-muscle myosin, and non-muscle tropomyosin (4, 20, 32). Therefore it is possible that results from immunoprecipitation analysis with #067 mAb would show associated molecules of S100A4; in fact we have previously expected molecular weight of #067 antigen as about 70 kDa higher than 10 kDa of S100A4. Evidence has also accumulated in support of the hypothesis that S100A4 can interact with p53 and affect p53-dependent pathways (3, 9, 25). Furthermore, it has been reported that S100A4 protein secreted from tumor cells can increase endothelial cell motility and hence induces angiogenesis (2). Despite this data, the precise function of this protein is still not fully known.

De Vouge et al. indicated that the S100A4 protein was up-regulated in some ras transformants (6). According to this report, S100A4 was definitely up-regulated in W31 cells, since W31 cells were H-ras transformants of WFB cells.

S100A4 is well known to have a secretory form via exocytosis, but to date, it is not known as a cell surface antigen. S100A4 protein has been shown to be localized along stress fibers, concentrated in the perinuclear region, or at membrane protrusions (21, 23, 30). However, our flow cytometry data suggested that S100A4 protein is present on the cell surface. Kislinger et al. indicated that a cell surface receptor, RAGE (receptor for advanced glycation end products), has the capacity to bind S100A4 on the cell surface of endothelial cells, monocyte/macrophages, smooth muscle cells, and neurons (18). Since rat brain tissue was well stained with #067 mAb (data not shown), WFB and W31 cells are possibly related to neurons in their characterization, although we did not confirm that RAGE existed on both cell types. Moreover, it was recently reported that in microarray experiments, expression of RAGE was found in some human tumors where abundant S100A4 and S100A6 expression were also observed (13). Therefore, we might expect to observe a complex of S100A4 protein and RAGE. Also intracellular Ca^{2+} concentration was found to be very important for the localization of the S100A4 protein. It was reported that up-regulated intracellular Ca^{2+} concentration relocated S100A4 protein from the perinuclear region towards the plasma membrane (28). Therefore, other than increased intracellular Ca^{2+} concentrations, it is also possible that alterations of microenvironment may also affect the localization of S100A4.

Our data suggests that S100A4 is a possible target for TCRγδ T cell-mediated lysis, though there is no report that S100A4 is a target molecule of TCRγδ T cells. In terms of antigen recognition, TCRγδ molecules are thought to be more similar to immunoglobulins (Igs) than TCRαβ molecules. It was reported that several TCRγδ molecules recognized protein molecules without processing, just like Igs. Previously published observations of TCRγδ T cell-mediated lysis indicated the involvement of several molecules such as mouse allo-MHC class II, or non-classical MHC class I and TL10, human MICA and MICB (10, 11, 29). Our results indicated that S100A4 may also play a role in TCRγδ T cell-mediated lysis.

In conclusion, the present study suggests that S100A4 protein and #067 antigen may be one and the same molecule. To our knowledge, this is the first report of a possible novel function of S100A4 in the

mechanism of TCRγδ T cell-mediated lysis. Further investigations will be required to understand the mechanism of S100A4 in relation to TCRγδ T cell-mediated lysis. This will also provide a basis for the ligands of TCRγδ T cells and the way to mediate the cell lysis.

This work was supported by Grants-in-Aid for Scientific Research from the Japan Society for the Promotion of Science to S. Ichimiya (No. 16590286) and N. Sato (No. 09470067 and No. 07457063).

References

1) Ambartsumian, N.S., Grigorian, M.S., Larsen, I.F., Karlstrom, O., Sidenius, N., Rygaard, J., Georgii, G., and Lukanidin, E. 1996. Metastasis of mammary carcinomas in GRS/A hybrid mice transgenic for the mts1 gene. Oncogene **13**: 1621–1630.
2) Ambartsumian, N.S., Klingelhofer, J., Grigorian, M.S., Christensen, C., Kriajevska, M., Tulchinsky, E., Georgiev, G., Berezin, V., Bock, E., Rygaard, J., Cao, R., Cao, Y., and Lukanidin, E. 2001. The metastasis-associated Mts1 (S100A4) protein could act as an angiogenic factor. Oncogene **20**: 4685–4695.
3) Chen, H., Fernig, D.G., Rudland, P.S., Sparks, A., Wilkinson, M.C., and Barraclough, R. 2001. Binding to intracellular targets of the metastasis inducing protein, S100A4 (p9Ka). Biochem. Biophys. Res. Commun. **286**: 1212–1217.
4) Davies, B.R., Davies, M.P., Gibbs, F.E., Barraclough, R., and Rudland, P.S. 1993. Induction of the metastatic phenotype by transfection of a benign rat mammary epithelial cell line with the gene for p9Ka, a rat calcium-binding protein, but not with the oncogene EJ-ras-1. Oncogene **8**: 999–1008.
5) Davies, M.P., Rudland, P.S., Robertson, L., Parry, E.W., Jolicoeur, P., and Barraclough, R. 1996. Expression of the calcium-binding protein S100A4 (p9Ka) in MMTV-neu transgenic mice induces metastasis of mammary tumours. Oncogene **13**: 1631–1637.
6) De Vouge, M.W., and Mukherjee, B.B. 1992. Transformation of normal rat kidney cells by v-K-ras enhances expression of transin 2 and an S100-related calcium-binding protein. Oncogene **7**: 109–119.
7) Donato, R. 1999. Functional roles of S100 proteins, calcium-binding proteins of the EF-hand type. Biochim. Biophys. Acta **1450**: 191–231.
8) Ford, H.L., Salim, M.M., Chakravarty, R., Aluiddin, V., and Zain, S.B. 1995. Expression of Mts1, a metastasis-associated gene, increases motility but not invasion of a non-metastatic mouse mammary adenocarcinoma cell line. Oncogene **11**: 2067–2075.
9) Grigorian, M., Andresen, S., Tulchinsky, E., Kriajevska, M., Carlberg, C., Kruse, C., Cohn, M., Ambartsumian, N., Christensen, A., Selivanova, G., and Lukanidin, E. 2001. Tumor suppressor p53 protein is a new target for the metastasis-associated Mts1/S100A4 protein. Functional consequences of their interaction. J. Biol. Chem. **276**: 22699–22708.
10) Groh, V., Steinle, A., Bauer, S., and Spies, T. 1998. Recognition of stress-induced MHC molecules by intestinal epithelial γδ T cells. Science **279**: 1737–1740.
11) Haas, W., Pereira, P., and Tonegawa, S. 1993. Gamma/delta T cells. Annu. Rev. Immunol. **11**: 637–686.
12) Heizmann, C.W., Fritz, G., and Schäfer, B.W. 2002. S100 proteins: structure, function and pathology. Front. Biosci. **7**: 1356–1368.
13) Hsieh, H.L., Schäfer, B.W., Sasaki, N., and Heizmann, C.W. 2003. Expression analysis of S100 proteins and RAGE in human tumors using tissue microarrays. Biochem. Biophys. Res. Commun. **307**: 375–381.
14) Ichimiya, S., Kojima, T., Momota, H., Kondo, N., Ozaki, T., Nakagawa, A., Toribio, M.L., Imamura, M., and Sato, N. 2002. p73 is expressed in human thymic epithelial cells. J. Histochem. Cytochem. **50**: 455–462.
15) Ichinohe, T., Ichimiya, S., Kishi, A., Tamura, Y., Kondo, N., Ueda, G., Torigoe, T., Yamaguchi, A., Hiratsuka, H., Hirai, I., Kohama, G., and Sato, N. 2003. T-cell receptor variable γ chain gene expression in the interaction between rat γδ-type T cells and heat shock protein 70-like molecule. Microbiol. Immunol. **47**: 351–357.
16) Kimura, K., Endo, Y., Yonemura, Y., Heizmann, C.W., Schafer, B.W., Watanabe, Y., and Sasaki, T. 2000. Clinical significance of S100A4 and E-cadherin-related adhesion molecules in non-small cell lung cancer. Int. J. Oncol. **16**: 1125–1131.
17) Kishi, A., Ichinohe, T., Hirai, I., Kamiguchi, K., Tamura, Y., Kinebuchi, M., Torigoe, T., Ichimiya, S., Kondo, N., Ishitani, K., Yoshikawa, T., Kondo, M., Matsuura, A., and Sato, N. 2001. The cell surface-expressed HSC70-like molecule preferentially reacts with the rat T-cell receptor Vγ6 family. Immunogenetics **53**: 401–409.
18) Kislinger, T., Fu, C., Huber, B., Qu, W., Taguchi, A., Yan, S.D., Hofmann, M., Yan, S.F., Pischetsrieder, M., Stern, D., and Schimid, A.M. 1999. N (epsilon)-(carboxymethyl) lysine adducts of proteins are ligands for receptor for advanced glycation end products that activate cell signaling pathways and modulate gene expression. J. Biol. Chem. **274**: 31740–31749.
19) Konno, A., Sato, N., Yagihashi, A., Cho, J., Torimoto, K., Hara, I., Wada, Y., Okubo, M., Takahashi, N., and Kikuchi, K. 1989. Heat- or stress-inducible tranaformation-associated cell surface antigen on the activated H-ras oncogene-transfected rat fibroblast. Cancer Res. **49**: 6578–6582.
20) Kriajevska, M.V., Cardenas, M.N., Grigorian, M.S., Ambartsumian, N.S., Georgiev, G.P., and Lukanidin, E.M. 1994. Non-muscle myosin heavy chain as a possible target for protein encoded by metastasis-related mts-1 gene. J. Biol. Chem. **269**: 19679–19682.
21) Kriajevska, M., Fischer-Larsen, M., Moertz, E., Vorm, O., Tulchinsky, E., Grigorian, M., Ambartsumian, N., and Lukanidin, E. 2002. Liprin 1, a member of the family of LAR transmembrane tyrosine phosphatase-interacting proteins, is a new target for the metastasis-associated protein S100A4 (mts1). J. Biol. Chem. **277**: 5229–5235.
22) Maelandsmo, G.M., Hovig, E., Skrede, M., Engebraaten, O., Florenes, V.A., Myklebost, O., Grigorian, M., Lukanidin, E., Scanlon, K.J., and Fodstad, O. 1996. Reversal of

the *in vivo* metastatic phenotype of human tumor cells by an anti-CAPL (mts1) ribozyme. Cancer Res. **56**: 5490–5498.

23) Mueller, A., Bächi, T., Höchli, M., Schäfer, B.W., and Heizmann, C.W. 1999. Subcellular distribution of S100 proteins in tumor cells and their relocation in response to calcium activation. Histochem. Cell Biol. **111**: 453–459.

24) Ninomiya, I., Ohta, T., Fushida, S., Endo, Y., Hashimoto, T., Yagi, M., Fujimura, T., Nishimura, G., Tani, T., Shimizu, K., Yonemura, Y., Heizmann, C.W., Schäfer, B.W., Sasaki, T., and Miwa, K. 2001. Increased expression of S100A4 and its prognostic significance in esophageal squamous cell carcinoma. Int. J. Oncol. **18**: 715–720.

25) Parker, C., Lakshmi, M.S., Piura, B., and Sherbet, G.V. 1994. Metastasis-associated mts1 gene expression correlates with increased p53 detection in the B16 murine melanoma. DNA Cell Biol. **13**: 343–351.

26) Parker, C., Whittaker, P.A., Usmani, B.A., Lakshmi, M.S., and Sherbet, G.V. 1994. Induction of 18A2/mts1 gene expression and its effects on metastasis and cell cycle control. DNA Cell Biol. **13**: 1021–1028.

27) Rudland, P.S., Platt-Higgins, A., Renshaw, C., West, C.R., Winstanley, J.H.R., Robertson, L., and Barraclough, R. 2000. Prognostic significance of the metastasis-inducing protein S100A4 (p9Ka) in human breast cancer. Cancer Res. **60**: 1595–1603.

28) Schild, H., Mavaddat, N., Litzenberger, C., Ehrich, E.W., Davis, M.M., Bluestone, J.A., Matis, L., Draper, R.K., and Chien, Y.H. 1994. The nature of major histocompatibility complex recognition by T cells. Cell **76**: 29–37.

29) Takashima, S., Sato, N., Kishi, A., Tamura, Y., Hirai, I., Torigoe, T., Yagihashi, A., Takahashi, S., Sagae, S., Kudo, R., and Kikuchi, K. 1996. Involvement of peptide antigens in the cytotoxicity between 70-kDa heat shock cognate protein-like molecule and CD3+, CD4−, CD8−, TCRαβ−, killer T cells. J. Immunol. **157**: 3391–3395.

30) Takenaga, K., Nakamura, Y., and Sakiyama, S. 1994. Cellular localization of pEL98 protein, an S100-related calcium binding protein, in fibroblasts and its tissue distribution analyzed by monoclonal antibodies. Cell Struct. Funct. **19**: 133–141.

31) Takenaga, K., Nakamura, Y., and Sakiyama, S. 1997. Expression of antisense RNA to S100A4 gene encoding an S100-related calcium-binding protein suppresses metastatic potential of high-metastatic Lewis lung carcinoma cells. Oncogene **14**: 331–337.

32) Takenaga, K., Nakamura, Y., Sakiyama, S., Hasegawa, Y., Sato, K., and Endo, H. 1994. Binding of pEL98 protein, an S100-related calcium binding protein, to nonmuscle tropomyosin. J. Cell Biol. **124**: 757–768.

33) Tamura, Y., Tsuboi, N., Sato, N., and Kikuchi, K. 1993. 70 kDa heat shock cognate protein is a transformation-associated antigen and a possible target for the host's antitumor immunity. J. Immunol. **151**: 5516–5524.

34) Yonemura, Y., Endou, Y., Kimura, K., Fushida, S., Bandou, E., Taniguchi, K., Kinoshita, K., Ninomiya, I., Sugiyama, K., Heizmann, C.W., Schäfer, B.W., and Sasaki, T. 2000. Inverse expression of S100A4 and E-cadherin is associated with metastatic potential in gastric cancer. Clin. Cancer Res. **6**: 4234–4242.

Developmental Cell, Vol. 7, 663–676, November, 2004, Copyright ©2004 by Cell Press

Polycomb Group Proteins Ring1A/B Link Ubiquitylation of Histone H2A to Heritable Gene Silencing and X Inactivation

Marlana de Napoles,[1] Jacqueline E. Mermoud,[1,5] Rika Wakao,[2,5] Y. Amy Tang,[1] Mitsuhiro Endoh,[2] Ruth Appanah,[1] Tatyana B. Nesterova,[1] Jose Silva,[1] Arie P. Otte,[3] Miguel Vidal,[4] Haruhiko Koseki,[2] and Neil Brockdorff[1,*]
[1]Developmental Epigenetics Group
MRC Clinical Sciences Centre
ICFM
Hammersmith Hospital
DuCane Road
London W12 ONN
United Kingdom
[2]Department of Developmental Genetics
RIKEN Research Center for Allergy and Immunology
RIKEN Yokohama Institute
1-7-22 Suehiro
Tsurumi-ku, Yokohama 230-0045
Japan
[3]Swammerdam Institute for Life Sciences
University of Amsterdam
Kruislaan 406
1098 SM Amsterdam
Holland
[4]Department of Developmental and Cell Biology
Centro de Investigaciones Biologicas
CSIC
Ramiro de Maeztu 9
28040 Madrid
Spain

Summary

In many higher organisms, 5%–15% of histone H2A is ubiquitylated at lysine 119 (uH2A). The function of this modification and the factors involved in its establishment, however, are unknown. Here we demonstrate that uH2A occurs on the inactive X chromosome in female mammals and that this correlates with recruitment of Polycomb group (PcG) proteins belonging to Polycomb repressor complex 1 (PRC1). Based on our observations, we tested the role of the PRC1 protein Ring1B and its closely related homolog Ring1A in H2A ubiquitylation. Analysis of Ring1B null embryonic stem (ES) cells revealed extensive depletion of global uH2A levels. On the inactive X chromosome, uH2A was maintained in Ring1A or Ring1B null cells, but not in double knockout cells, demonstrating an overlapping function for these proteins in development. These observations link H2A ubiquitylation, X inactivation, and PRC1 PcG function, suggesting an unanticipated and novel mechanism for chromatin-mediated heritable gene silencing.

*Correspondence: neil.brockdorff@csc.mrc.ac.uk
[5]These authors contributed equally to this work.

Introduction

The histone code hypothesis proposes that covalent modifications of specific residues provide interaction surfaces for proteins that either increase or decrease chromatin accessibility and that this in turn impacts on the regulation of transcription, replication, and chromosome behavior (Strahl and Allis, 2000; Jenuwein and Allis, 2001). Considerable progress has been made in identifying key modifications such as acetylation, methylation, phosphorylation, and ubiquitylation and in determining their association with either open (eu-) chromatin or repressed (hetero-) chromatin states (reviewed in Turner, 2002). In many cases, enzymes/complexes have been identified that either add or remove specific modifications, for example histone acetylases (HATs), histone deacetylases (HDACs), and histone methyltransferases (HMTases). In addition, proteins or domains have been identified that recognize and bind modified histone surfaces: for example, heterochromatin protein 1 (HP1), which is implicated in defining or perpetuating a hetereochromatic structure, recognizes histone H3 di- or trimethylated at lysine (K) 9 (Lachner et al., 2001; Bannister et al., 2001). In addition to the role of modifications at individual sites, synergism between different modifications is also key in terms of defining function. An example of this is provided by the requirement for H2B ubiquitylation for H3-K4 and H3-K79 methylation in *S. cerevisiae* (Sun and Allis, 2002; Dover et al., 2002; Briggs et al., 2002).

The function of some histone modifications has not yet been determined. A notable example is ubiquitylation of histone H2A, which occurs at lysine 119 in many but not all higher eukaryotes (Goldknopf et al., 1975; Nickel and Davie, 1989). Ubiquitylated H2A (uH2A) has been estimated to comprise between 5% and 15% of the available H2A and is therefore a relatively abundant modification. However, there is contradictory evidence concerning its function. Some studies have pointed to an association of uH2A with transcriptionally active chromatin (Levinger and Varshavsky, 1982; Nickel et al., 1989). Others, however, have failed to demonstrate such a link (Huang et al., 1986; Parlow et al., 1990; Dawson et al., 1991). Moreover, Baarends et al. (1999) reported that uH2A is abundant in mouse pachytene spermatocytes and is enriched on the transcriptionally silent XY body.

Genetic screens in *D. melanogaster* identified the Polycomb group (PcG) and Trithorax group (TrG) of proteins as memory factors involved, respectively, in heritable silencing and heritable activation of homeotic genes. A number of PcG proteins have been assigned to one of two large multiprotein complexes. In *D. melanogaster*, the 2 MDa PRC1 complex contains stoichometric amounts of Polyhomeotic (PH), Polycomb (PC), Posterior sex combs (PSC), and dRING (Shao et al., 1999; Francis et al., 2001), and the 600 kDa PRC2 complex contains ESC, E(Z), and SU(Z)12 (Muller et al., 2002). In

mammals, the same two complexes have been identified, although there are multiple homologs for each of the PRC1 PcG proteins.

The PRC2 complex has been shown to catalyze trimethylation of histone H3-K27 (Czermin et al., 2002; Muller et al., 2002; Cao et al., 2002; Kuzmichev et al., 2002; Fischle et al., 2003; Min et al., 2003). Interestingly, the PRC1 protein Polycomb (PC) has a chromodomain that recognizes trimethylated H3-K27 (tri-meH3-K27) (Cao et al., 2002; Kuzmichev et al., 2002; Fischle et al., 2003; Min et al., 2003), and it has been suggested that this interaction could result in recruitment of PRC1 complexes to PRC2 targets. The molecular mechanism of PRC1 function is poorly understood but is thought to involve inhibition of SWI/SNF chromatin remodeling (Shao et al., 1999). Two of the core PRC1 proteins, PSC and dRING, have a Ring finger domain. This motif is characteristic of ubiquitin and SUMO E3 ligases (reviewed in Pickart, 2001).

Model systems that have been useful in unraveling the links between histone modifications and biological function include well-studied gene loci (for example, the α- and β-globin gene clusters) and regions comprising either constitutive heterochromatin (for example, centromeres and telomeres) or facultative heterochromatin, in particular the inactive X chromosome (Xi) in female mammals. In this latter example, there is a developmentally regulated and stepwise conversion of an entire X chromosome from a euchromatic to a heterochromatic conformation (reviewed in Heard, 2004). The process is triggered by the expression and in *cis* localization of a large noncoding RNA, the X inactive specific transcript (*Xist*) (Brown et al., 1991, 1992; Brockdorff et al., 1992). *Xist* RNA is thought to elicit chromosome silencing by recruiting chromatin-modifying factors. Consistent with this, recent studies have demonstrated that *Xist* RNA recruits PRC2 PcG complexes with resultant chromosome-wide H3-K27 trimethylation (Mak et al., 2002; Silva et al., 2003; Plath et al., 2003; Kohlmaier et al., 2004). This in turn has been shown to be required for stable long-term maintenance of X inactivation (Wang et al., 2001; Silva et al., 2003).

In this study, we demonstrate that a subset of PRC1 proteins, including the Ring finger proteins Mel18 and Ring1B, are transiently enriched on Xi in early development. Additionally, we show that Xi is highly enriched for uH2A and that this occurs coincident with PRC1 complex recruitment. Analysis of cells lacking Ring1B and the highly similar Ring1A proteins demonstrates that Ring1B is required to maintain global uH2A levels in ES cells and that Ring1A and Ring1B have an overlapping function in maintaining uH2A on Xi in differentiated cells. We discuss these results in the context of understanding the mechanism of action and evolution of PRC1 PcG proteins.

Results

Recruitment of PRC1 PcG Proteins to the Inactive X Chromosome

It has been proposed that the PRC1 and PRC2 PcG complexes are recruited to common sites as a result of an interaction between the chromodomain of the PRC1 protein PC and H3-K27 trimethylation (tri-meH3-K27) catalyzed by the PRC2 HMTase, EZ (Czermin et al., 2002; Muller et al., 2002; Cao et al., 2002; Kuzmichev et al., 2002; Fischle et al., 2003; Min et al., 2003). In a previous study, we reported that PRC2 is recruited to Xi in early development and that it is required to establish trimeH3-K27 on Xi (Silva et al., 2003). However, we failed to detect enrichment of the PRC1 proteins Bmi1, Mpc2, or Ring1A either in early embryogenesis or at later stages (Mak et al., 2002; Silva et al., 2003). Because mammals have at least two homologs of each of the core PRC1 proteins, we extended this initial study using antisera specific to Ring1B, Mel18, Mph1, and Mph2. We first carried out immunofluorescence analysis on XX trophoblast stem (TS) cells, a model system for the imprinted X inactivation that occurs in extraembryonic tissues in mouse (Mak et al., 2002). Using antisera to the PRC2 proteins Suz12 or Eed to identify Xi domains, we observed Xi enrichment of Ring1B (Figure 1A) and also Mel18 and Mph2 (not shown). Scoring data illustrates that Ring1B enrichment on Xi is seen in the majority of cells, whereas Mel18, and in particular Mph2 enrichment, is less frequent (Figure 1A, graph).

We went on to determine if PRC1 enrichment on Xi occurs during in vitro differentiation of XX embryonic stem (ES) cells. This model system is representative of the random X inactivation that occurs in cells of the embryo proper and provides a useful means to analyze the dynamics of different steps of the X inactivation process. Previous studies have demonstrated that X inactivation proceeds in an ordered and stepwise process following the onset of *Xist* expression (reviewed in Heard, 2004). Recruitment of PRC2 proteins and consequent H3-K27 trimethylation is one of the earliest detectable changes. At later differentiation stages, Xi enrichment of PRC2 proteins is markedly reduced but H3-K27 trimethylation is retained (Silva et al., 2003; Plath et al., 2003). As shown in Figure 1B, a similar pattern was observed for the PRC1 proteins Ring1B, Mel18, and Mph1. Thus, recruitment to Xi occurs rapidly during early differentiation, but enrichment is undetectable at later differentiation stages. These findings suggest that a PRC1-like complex is recruited to Xi during the onset of X inactivation. The complex appears to utilize the homologous Mph1 and Mph2 proteins differently in TS cells compared with ES cells, suggesting that its composition may vary in a tissue-specific manner.

We went on to test if PRC1 protein enrichment on Xi occurs at the onset of X inactivation in early mouse embryos. Detection of the PRC2 protein Suz12 was used to identify Xi domains in XX embryos. A first wave of inactivation, initiated in early preimplantation embryos, results in imprinted inactivation of the paternal X chromosome (Xp) in all cells of late morula and early blastocyst stage embryos (Okamoto et al., 2004; Mak et al., 2004). We observed Ring1B localizing to Xi domains both in trophectoderm and ICM regions of early blastocyst stage embryos (Figure 1C), indicating that PRC1 recruitment occurs during imprinted X inactivation in vivo. Imprinted X inactivation is reversed in cells allocated to the pluripotent epiblast lineage at the late blastocyst stage, setting the scene for subsequent random X inactivation in the embryo proper at approximately 6

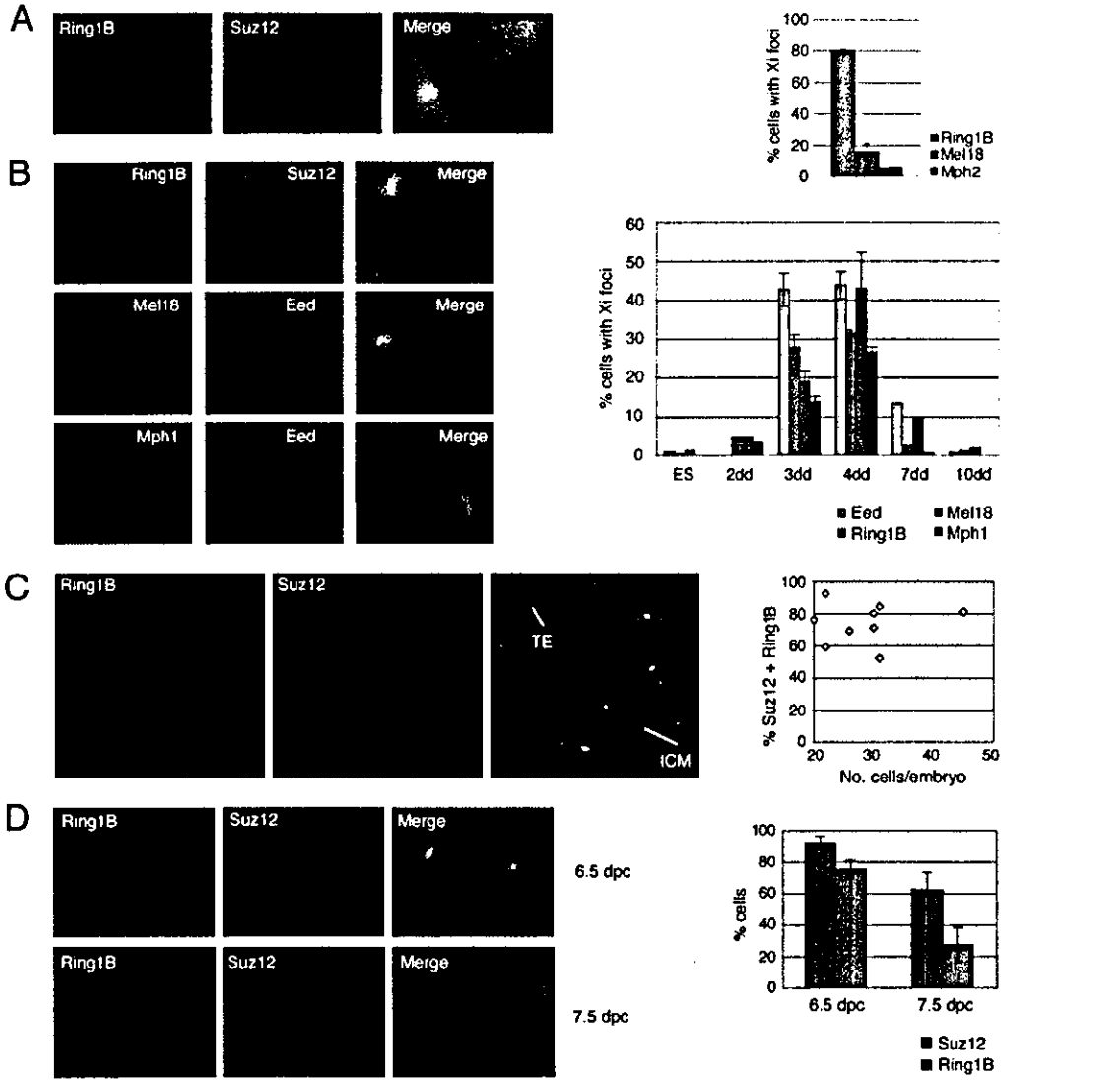

Figure 1. Enrichment of PRC1 Proteins on the Inactive X Chromosome

(A) Example of immunofluorescence analysis in TS cells showing colocalization of Ring1B and Suz12 in Xi domains. Quantitative scoring data (graph) shows colocalization with Suz12 domains for Ring1B (n = 289), Mel18 (n = 405), and Mph2 (n = 100). Error bars indicate variation between different slides.

(B) Examples of immunofluorescence analysis of differentiating PGK12.1 XX ES cells illustrating Xi enrichment of the PRC1 proteins Ring1B (top), Mel18 (center), and Mph1 (bottom). Scoring data (graph) illustrates the proportion of cells with Xi foci detected with antibodies to Eed, Ring1B, Mel18, and Mph1 in undifferentiated cells (ES) and for cells differentiated for 2–10 days (dd). A minimum of 207 cells were scored for each point. Error bars show variation between individual slides.

(C) Example of immunofluorescence analysis illustrating Ring1B localization to Xi domains in an XX blastocyst stage embryo. The image represents a single confocal section. Xi localization was observed in cells in the trophectoderm (TE) and inner cell mass (ICM) regions. The scatterplot shows the number of cells with Ring1B colocalizing with Suz12 domains plotted against the number of cells in a series of individual XX blastocyst stage embryos.

(D) Examples of immunofluorescence analysis illustrating Ring1B localization to Xi domains in XX postimplantation embryos isolated at 6.5 and 7.5 dpc. Scoring data (graph) shows the proportion of cells with Xi domains for Suz12 and Ring1B at 6.5 dpc (312 cells from 4 embryos) and 7.5 dpc (884 cells from 4 embryos). Error bars indicate variation between individual embryos.

days postcoitum (dpc). Consistent with this, we observed Xi localization of Ring1B in the majority of cells at 6.5 dpc (Figure 1D). At 7.5 dpc, there was a marked reduction, paralleling reduced enrichment of the PRC2 protein Suz12 on Xi. At 11.5 dpc, we failed to detect any localization to Xi domains (not shown). This progressive loss of Ring1B enrichment on Xi mirrors the results obtained for differentiating XX ES cells.

Ubiquitylation of Histone H2A on the Inactive X Chromosome

Both Mel18 and Ring1B proteins have Ring finger domains, indicating that they function either in ubiquitylation or sumolyation pathways. We therefore carried out immunostaining experiments to determine if either SUMO or ubiquitin groups are enriched on Xi. In initial experiments, we analyzed XX TS cells. To test if the Xi domain is enriched for ubiquitin, we used an antibody, FK2, which detects both mono- and polyubiquitin chains (Fujimuro et al., 1994). No Xi-specific signal was detected under conditions where cells are first fixed and then permeabilized (not shown). However, by reversing these two steps, a clear signal that colocalized with Xi was seen in all cells (Figure 2A). To discriminate between mono- and polyubiquitylated proteins, we used the FK1 antibody, which is specific for polyubiquitylated proteins (Fujimuro et al., 1994). Here, we also observed Xi signal but it was significantly weaker and was detectable in only 22% of cells (Figure 2B). Thus, both mono- and polyubiquitylated protein(s) are enriched in Xi domains but monoubiquitylated protein(s) predominate. No Xi signal was seen using antibodies to SUMO1 (not shown).

The stringent conditions required to expose the ubiquitin signal on Xi suggested that the epitope may be partially occluded. This, in turn, led us to consider that ubiquitylation may be occurring on a histone protein. The core histones H2A, H2B, and H3 and also histone H1 are all known to be subject to ubiquitylation (reviewed in Zhang, 2003). Ubiquitylated H2A (uH2A) represented a good candidate, as it is relatively abundant in higher eukaryotes, comprising 5%–15% of the total H2A. Availability of a highly specific monoclonal antibody (Vassilev et al., 1995) allowed us to test this hypothesis. As shown in Figure 2C, we observed a strong and highly specific staining of Xi domains in all cells. Thus, uH2A is highly enriched on Xi, providing a strong indication that this histone modification is associated with transcriptionally silent facultative heterochromatin. A fraction of uH2A has been reported to be polyubiquitylated (Nickel and Davie, 1989), possibly explaining the Xi staining seen with FK1 antibody (Figure 2B).

Although the uH2A staining pattern indicates that Xi is the major target site in XX TS cells, this strong signal masks a more general nuclear localization. This can be seen in immunofluorescence analysis of XY TS cells, where signal is detectable throughout the nucleoplasm except in nucleoli and DAPI-dense regions (Figure 2D). The latter observation indicates that H2A ubiquitylation is not a feature of constitutive heterochromatin. Western blot analysis shows that overall levels of uH2A are very similar in XX and XY TS cells (Figure 2E), suggesting that the contribution of uH2A on Xi is relatively small. We conclude from this that most uH2A is associated with sites dispersed throughout the genome.

Kinetics of H2A Ubiquitylation on the Inactive X Chromosome

To test for H2A ubiquitylation in random X inactivation and to examine the dynamics of this modification, we analyzed differentiating XX ES cells (Figure 3A). For these experiments, Xi domains were identified using

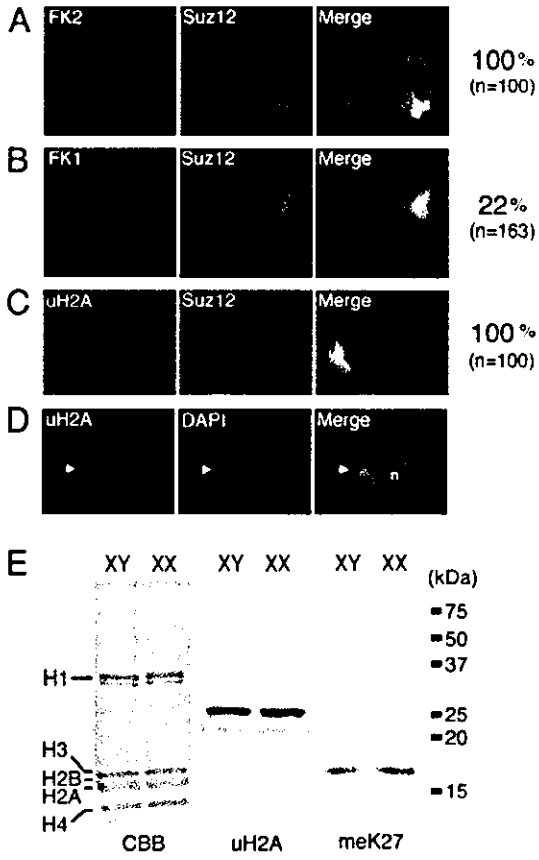

Figure 2. Ubiquitylated Histone H2A Is Highly Enriched on the Inactive X Chromosome in TS Cells

(A) Example of immunofluorescence analysis with FK2 antibody, which detects both mono- and polyubiquitylated proteins, illustrating strong Xi signal that was seen in all cells with Su(z)12 Xi foci.
(B) Example of immunofluorescence analysis using FK1 antibody, which detects only polyubiquitylated proteins, showing that Xi staining is relatively weak and is seen only in a proportion of cells.
(C) Example of immunofluorescence analysis for ubiquitylated H2A (uH2A), showing localization to Xi in all cells with Su(z)12 Xi foci.
(D) Example of immunofluorescence analysis illustrating nuclear staining of uH2A in XY TS cells. Staining is excluded from nucleoli (n) and DAPI-dense pericentric heterochromatin (arrowhead).
(E) Western blot analysis of acid-extracted histones from XY and XX TS cells. The figure shows Coomassie brilliant blue staining of acid-extracted histones (CBB, left) and Western blot analysis using antibody to ubiquitylated H2A (uH2A, center) or trimethylated H3-K27 (meK27, right).

antibodies to tri-meH3-K27. This provided a more reliable marker of Xi under the stringent conditions used to detect uH2A. As illustrated, H2A ubiquitylation detected with either FK2 or uH2A antibodies occurred with similar kinetics to PRC2-catalyzed H3-K27 trimethylation and PRC1 protein recruitment. Interestingly, uH2A on Xi was detectable on metaphase chromosomes, showing a banded pattern that colocalizes with tri-meH3-K27 (Figure 3A, lower panels). This pattern has been shown to relate to preferential localization of *Xist* RNA in gene-rich G-light bands (Duthie et al., 1999).

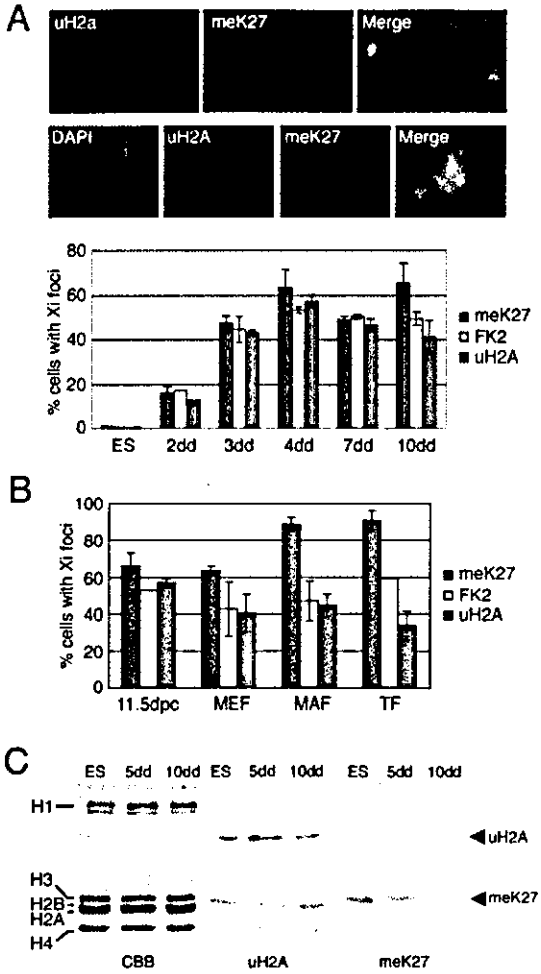

Figure 3. H2A Ubiquitylation in Random X Inactivation

(A) Examples of immunofluorescence analysis illustrating ubiquitylated H2A (uH2A) and trimethylated H3-K27 (meK27) on Xi in differentiated ES cells at interphase (top) and on an individual Xi chromosome at metaphase (bottom). Scoring data (graph) illustrates differentiation-linked increase in uH2A on Xi, assessed both with uH2A and FK2 antibodies. The kinetics of H2A ubiquitylation closely mirrors that seen for trimethylation of H3-K27 (meK27). A minimum of 229 cells were scored for each point. Error bars indicate variation between slides.

(B) Graph illustrates data for various differentiated XX cell types: 11.5 dpc embryos, primary mouse embryo fibroblasts (MEF), primary mouse adult fibroblasts (MAF), and transformed fibroblast (TF) cell lines. The proportion of cells with Xi foci was scored using antibodies to tri-meH3-K27 (meK27) and to uH2A (FK2 and uH2A). A minimum of 193 cells were scored for each point. Error bars indicate variation between different slides.

(C) Western blot analysis of acid-extracted histones from undifferentiated PGK12.1 XX ES cells and from cells differentiated in vitro for 5 or 10 days (dd). The figure shows Coomassie brilliant blue staining of acid-extracted histones (CBB, left) and Western blot analysis using antibody to monoubiquitylated H2A (uH2A, center) or trimethylated H3-K27 (meK27, right).

Analysis of later stages of ES cell differentiation illustrates that uH2A enrichment is maintained on Xi beyond the time when PRC1 protein enrichment is detectable (compare Figures 1B and 3A graphs). Similarly, we observed uH2A on Xi in XX embryos at 11.5 dpc and in primary and transformed XX cell lines representing differentiated tissues (Figure 3B). We cannot rule out the possibility that relatively low levels of Ring1B, Mel18, and Mph1/2, or for that matter other PRC1 proteins, are associated with Xi in these situations.

Global levels of uH2A are similar in undifferentiated ES cells compared with cells differentiated for various times, contrasting with tri-meH3-K27, which is markedly elevated in undifferentiated ES cells (Figure 3C). The latter observation is consistent with previous studies demonstrating elevated PRC2 and tri-meH3-K27 both in ES cells and in the ICM of blastocyst stage embryos (Silva et al., 2003; Erhardt et al., 2003; Mak et al., 2004).

Differentiation Linked Stabilization of uH2A on the Inactive X Chromosome

To further examine the relationship between H2A ubiquitylation and the onset of X inactivation, we analyzed XY ES cell lines expressing an inducible *Xist* transgene. Previous studies have shown that expression of *Xist* transgenes in undifferentiated ES cells is sufficient to induce gene silencing and many of the chromatin modifications associated with X inactivation (Wutz and Jaenisch, 2000; Kohlmaier et al., 2004). We assayed *Xist* expression, recruitment of PRC2 (Suz12), PRC1 (Ring1B), H3-K27 trimethylation, and H2A ubiquitylation 72 hr following induction of *Xist* RNA in two independently derived ES cell lines, 8A and 12E (Figure 4A). Accumulation of *Xist* RNA into large nuclear domains occurred in the majority of cells in both cell lines. Recruitment of Suz12 and Ring1B and trimethylation of H3-K27 occurred in a reduced proportion of cells. Most strikingly, H2A ubiquitylation was detectable only in a very small proportion of cells.

Chromosome inactivation is unstable and *Xist* RNA dependent in undifferentiated ES cells and also during early differentiation stages, whereas in more differentiated cells, silencing is stabilized and becomes *Xist* independent (Wutz and Jaenisch, 2000). To determine if H2A ubiquitylation correlates with stabilization of inactivation, we assayed 8A and 12E cell lines during in vitro differentiation. *Xist* RNA expression was again induced for 72 hr, but under culture conditions where cell differentiation is allowed to proceed (Figure 4B). Recruitment of Suz12 and Ring1B was seen to increase relative to undifferentiated ES cells, as did H3-K27 trimethylation. The most dramatic difference, however, was seen for H2A ubiquitylation, which was now detectable in a similar proportion of cells as H3-K27 trimethylation (compare Figures 4A and 4B graphs). These observations indicate that cellular differentiation enhances both H3-K27 trimethylation and in particular H2A ubiquitylation occurring in response to *Xist* RNA accumulation. The fact that these histone modifications are relatively unstable in undifferentiated ES cells may be significant in relation to the reversibility of chromosome inactivation.

Ring1B Is Required for H2A Ubiquitylation in ES Cells

The correlation between H2A ubiquitylation and the recruitment of Ring finger proteins of the PRC1 complex

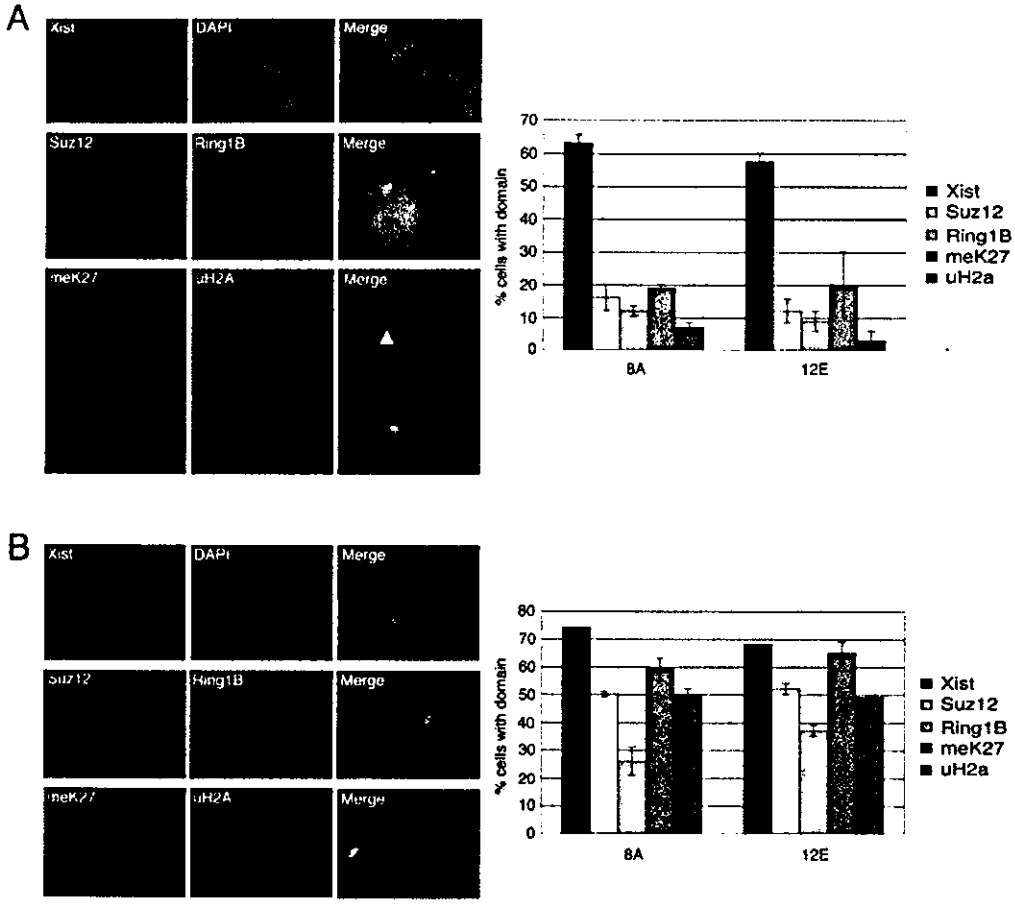

Figure 4. Ubiquitylated H2A on Xi Is Stabilized by Cellular Differentiation

(A) Examples showing *Xist* RNA FISH (top), immunofluorescence detection of Suz12 and Ring1B (center), and immunofluorescence detection of tri-meH3-K27 (meK27) and uH2A (bottom) in undifferentiated transgenic 8A ES cells 72 hr after *Xist* induction. Arrowhead illustrates a cell with a tri-meH3-K27 domain and no corresponding uH2A signal. Graph shows the proportion of cells with domains for each marker ($n > 200$), both for cell line 8A and the independently derived cell line 12E. Error bars indicate variation between different slides.

(B) Analysis of differentiating cells 72 hr after *Xist* induction, as in (A). Examples shown are from the 8A cell line.

to Xi suggested that these events may be directly linked. Ring1B in particular represented a good candidate, as previous studies have shown that null alleles result in early embryo lethality (Voncken et al., 2003; M.V. and H.K., unpublished). To test this, we analyzed the effect of Ring1B deficiency on H2A ubiquitylation. Because of embryonic lethality in Ring1B null animals, we used a conditional gene targeting strategy in which exon 2, encoding the ATG initiation codon, is flanked with loxP sites (Figure 5A). Two independently derived ES cell lines, 10-3 and 13-3, which are homozygous for the conditionally targeted allele (Ring1B$^{fl/fl}$), were used in this study. 10-3 cells were found to be XY based on PCR analysis of the Y-linked *Sry* gene (data not shown). 13-3 cells were *Sry* negative, indicating they are either XX or X0. Ring1B null (Ring1B$^{-/-}$) derivatives of both cell lines were obtained by CRE-mediated excision of exon 2.

We went on to analyze global ubiquitylated H2A levels in nuclear extracts before and after deletion of the locus. As shown in Figure 5B, loss of functional Ring1B resulted in a striking depletion of uH2A in both cell lines. Similar results were obtained by analyzing acid-extracted histones (Figure 5C, center). A low level of uH2A was observed in this experiment, possibly due to expression of the highly related Ring1A protein (see below). H3-K27 trimethylation levels were essentially unaffected (Figure 5C, right), demonstrating that depletion of uH2A is a highly specific effect and is not due to a more general disruption of chromatin structure.

To test if depletion of global uH2A levels is a direct consequence of mutating Ring1B, we carried out a complementation experiment, transfecting mutant ES cells with a construct expressing wild-type Ring1B from a heterologous chicken β-actin promoter. As shown in Figure 5D, the transfected mutant ES cells express high levels of transgene-encoded Ring1B protein. Analysis of acid-extracted histones demonstrated that uH2A levels

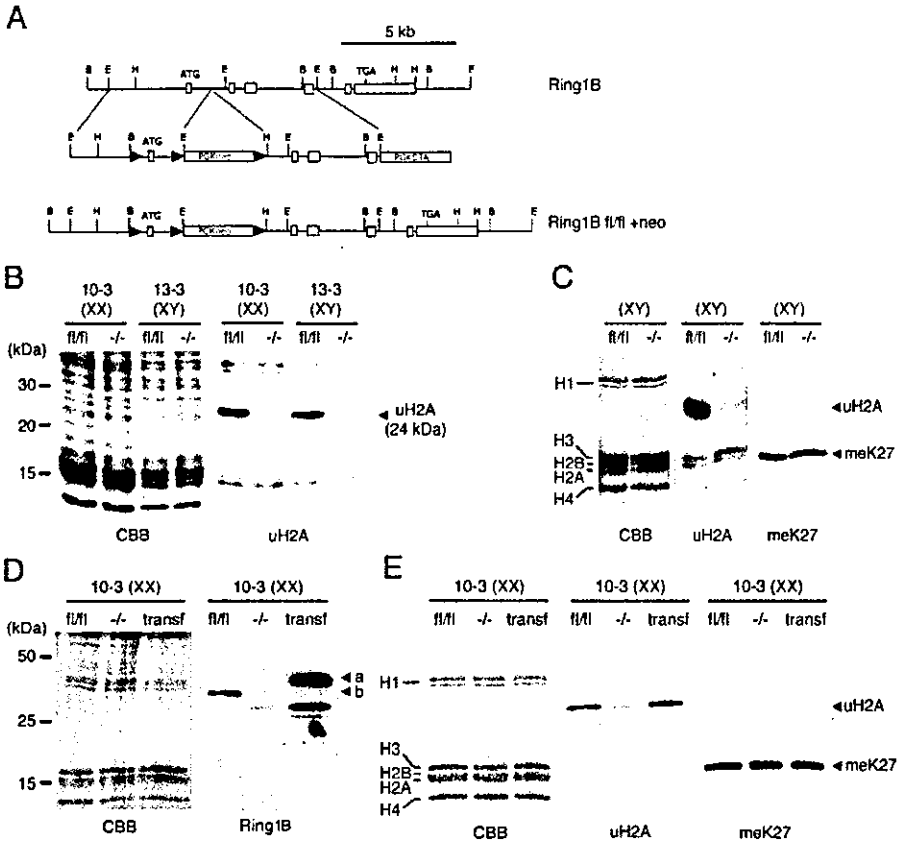

Figure 5. Ring1B Is Required for H2A Ubiquitylation in ES Cells

(A) Schematic restriction enzyme map illustrating the strategy for conditional targeting of the Ring1B locus. The targeting construct introduces loxP sites (filled triangles) flanking exon (open rectangles) 2 of the gene, containing the ATG initiation codon. An additional loxP site provides a means to delete the positive selectable marker gene, PGKneo. The termination codon TGA is also indicated. A cassette encoding diptheria toxin expressed from the PGK promoter (PGKDTA) was used to negatively select for random integrants. Restriction enzymes are BglII (B), EcoRI (E), and HindIII (H).

(B) Western blot analysis of uH2A in nuclear extracts from Ring1B$^{fl/fl}$ (fl/fl) and derivative Ring1B$^{-/-}$ (-/-) 10-3 and 13-3 undifferentiated ES cell lines. Coomassie brilliant blue (CBB) staining of extracts with molecular weights in kDa illustrated to the left.

(C) Western blot analysis of uH2A and tri-meH3-K27 (meK27) in acid-extracted histones from 13-3 cell lines. Positions of histones H1, H2A, H2B, H3, and H4 are indicated to the left of Coomassie brilliant blue (CBB) stained gel image.

(D and E) Complementation analysis of Ring1B$^{-/-}$ ES cells.

(D) Western analysis of Ring1B protein expression in nuclear extracts from XX 10-3 Ring1b$^{fl/fl}$ cells (fl/fl), Ring1b$^{-/-}$ derivatives (-/-), and Ring1b$^{-/-}$ cells after transfection with the Ring1B-myc construct (transf). Coomassie brilliant blue (CBB) staining with molecular weights indicated in kDa is shown in the left panel. The epitope-tagged protein (arrowhead a) migrates more slowly than wild-type protein (arrowhead b).

(E) Western analysis of acid-extracted histones from cell lines in (D) showing detection of both uH2A and tri-meH3-K27 (meK27). Coomassie brilliant blue (CBB) staining and indication of the position of histones is shown in the left panel.

are restored to a similar level to the parent Ring1B$^{fl/fl}$ cells (Figure 5E). These results confirm that Ring1B has a direct involvement in H2A ubiquitylation in ES cells.

Functional Redundancy of Ring1A and Ring1B in X Inactivation

Karyotypic anaylsis of the putative XX cell line 13-3 revealed that the majority of cells are tetraploid with three X chromosomes (not shown). Theoretically, these cells should initiate inactivation of at least one of their three X chromosomes upon differentiation. Analysis of *Xist* RNA expression demonstrated that this is the case, although the onset of expression occurred relatively late compared with other XX ES cell lines, between 4 and 11 days of differentiation, and was seen only in a small proportion of cells (Figure 6A, graph). This was also the case for the parent Ring1B$^{fl/fl}$ cell line, indicating that it represents a property of the parent cell line, rather than a consequence of Ring1B mutation (not shown). We went on to analyze Xi H3-K27 trimethylation and H2A ubiquitylation in these cells (Figure 6A). In all cases where Xi domains could be identified by tri-meH3-K27 staining, we also detected colocalizing uH2A signal. The frequency of positive cells was similar to the proportion of cells expressing *Xist* RNA.

A possible explanation for the occurrence of uH2A on

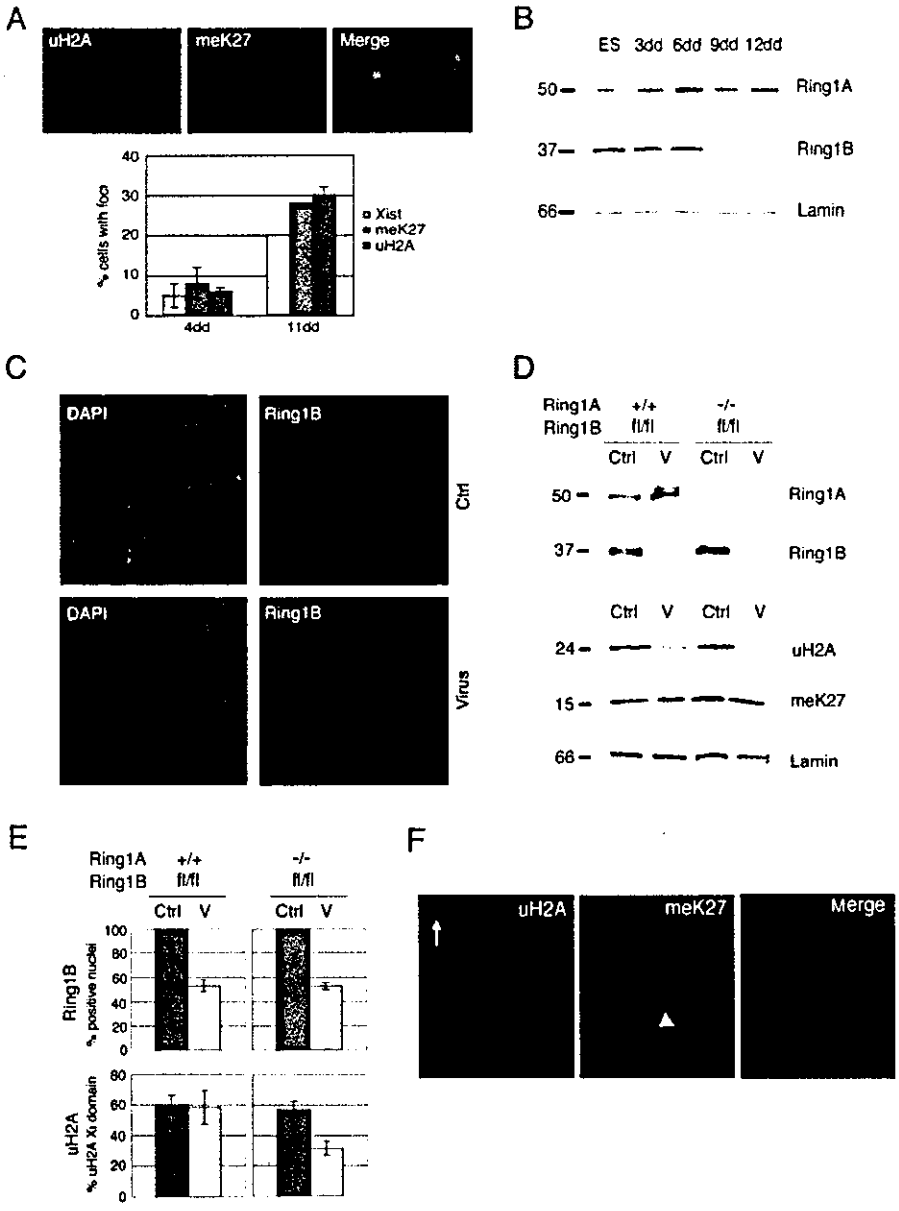

Figure 6. Overlapping Function of Ring1B and Ring1A in H2A Ubiquitylation on Xi

(A) Example of immunofluorescence analysis illustrating colocalizing uH2A and tri-meH3K27 (meK27) signals on Xi in 10-3 Ring1B$^{-/-}$ ES cells after 11 days of differentiation. Graph illustrates scoring data showing the proportion of cells with Xi foci for *Xist* RNA, tri-meH3-K27 (meK27), and uH2A after 4 and 11 days differentiation (dd).

(B) Western blot analysis showing expression profiles for Ring1B and Ring1A proteins in PGK12.1 XX ES cells and after in vitro differentiation for 3, 6, 9, and 12 days (dd). Molecular weights in kDa are indicated to the left. Detection of LaminB protein was used as a loading control.

(C) Example showing immunofluorescence detection of Ring1B in 2-8 MEF cells (Ring1A$^{-/-}$; Ring1B$^{fl/fl}$) without or with Ad-Cre virus treatment (Ctrl and Virus, respectively).

(D) Top panels show Western blot analysis for Ring1A and Ring1B in extracts from 1-4 MEF cells (Ring1A$^{+/+}$; Ring1B$^{fl/fl}$), and 2-8 MEF cells (Ring1A$^{-/-}$; Ring1B$^{fl/fl}$) either without (Ctrl) or with (V) Ad-Cre treatment. Lower panels show Western analysis of uH2A and tri-meH3-K27 (meK27). Molecular weights in kDa are indicated on the left. Detection of LaminB protein was used as a loading control.

(E) Upper graphs illustrate the proportion of 1-4 MEF cells (Ring1A$^{+/+}$; Ring1B$^{fl/fl}$) and 2-8 MEF cells (Ring1A$^{-/-}$; Ring1B$^{fl/fl}$) showing nuclear Ring1B staining without (Ctrl) or with (V) AdCre treatment. Lower graphs show the proportion of cells with uH2A Xi foci. Data for each point was compiled from scoring a minimum of 1167 cells on a total of four slides. Error bars illustrate variation between slides.

(F) Example of immunofluorescence analysis for uH2A and tri-meH3-K27 (meK27) in 2-8 cells (Ring1A$^{-/-}$; Ring1B$^{fl/fl}$) following Ad-Cre treatment. Arrow indicates a single cell with uH2A still present. Other cells lack detectable uH2A. Arrowhead indicates tri-meH3-K27 on Xi in one of these cells.

Xi in differentiated Ring1B$^{-/-}$ cells is functional redundancy with the highly similar Ring1A protein. Consistent with this, Western blot analysis reveals Ring1A expression in ES cells and differentiated derivatives. Ring1B expression, in contrast, is reduced in more differentiated cells (Figure 6B).

To analyze possible redundancy of Ring1A and Ring1B, we derived cell lines lacking both proteins. Ring1B deficiency results in early embryonic lethality, but Ring1A null animals are viable, and we were therefore able to derive Ring1A-deficient XX primary mouse embryo fibroblasts (MEF) homozygous for the conditional Ring1B^{fl} allele (primary cell line 2-8). As a control, we derived XX MEFs homozygous for Ring1B^{fl} on a wild-type Ring1A background (primary cell line 1-4). Subsequent deletion of Ring1B was achieved by infection of MEF cultures with adenovirus expressing CRE recombinase (Ad-Cre). Typical infection rates, as assessed by immunfluorescence detection of Ring1B protein, varied from 50% to 70% of cells (see Figure 6C for example). Ring1B depletion was clearly evident in Western analysis of infected cell cultures, as was depletion of global uH2A levels (Figure 6D). Interestingly, uH2A depletion appeared to be more marked in 2-8 cells lacking both Ring1A and Ring1B, consistent with an overlapping function for these proteins.

We went on to analyze uH2A on Xi. In control experiments, we noted that Ring1B$^{-/-}$ MEF cells are selected against during continuous culture and that this occurs predominantly between days 3 and 5 (data not shown). With this in mind, we analyzed cells 2 days after Ad-Cre infection, allowing sufficient time to detect effects on uH2A levels prior to the occurrence of cell selection. Figure 6E summarizes the results from two independent experiments. Examples are shown in Figure 6F. Approximately 50% of cells in 1-4 and 2-8 cultures treated with Ad-Cre were seen to lack Ring1B protein, as assessed by immunofluorescence (Figure 6E, top). In 1-4 cells (Ring1A$^{+/+}$; Ring1B$^{fl/fl}$), uH2A on Xi was detectable in approximately 60% of cells both in Ad-Cre-treated and untreated cultures (Figure 6E, bottom left). This result, demonstrating maintenance of uH2A on Xi in Ring1B null cells, is consistent with that obtained for the Ring1B null differentiated XX ES cell cultures (Figure 6A).

In 2-8 cells (Ring1A$^{-/-}$; Ring1B$^{fl/fl}$), we again observed uH2A on Xi at normal levels prior to Ad-Cre treatment. This indicates that deletion of Ring1A alone does not affect H2A ubiquitylation on Xi. However, in virus-treated cultures, we observed that the number of cells with uH2A staining on Xi is reduced by approximately 50%, similar to the proportion of cells in which Ring1B is deleted (Figure 6E, bottom right). Thus, uH2A on Xi can be maintained in cells lacking Ring1A or Ring1B but not in cells lacking both proteins. *Xist* RNA expression and triMeH3-K27 on Xi were unaffected in Ad-Cre-treated compared with untreated cultures (data not shown), indicating that depletion of uH2A on Xi is a direct effect of the combined deletion of Ring1A and Ring1B.

H2A Ubiquitylation and PRC1 Proteins in Evolution

H2A ubiquitylation is known to occur in many but not all eukaryotic organisms. A well-documented exception is the yeast *S. cerevisiae* (Robzyk et al., 2000). *S. cerevisiae* also has no direct homologs of PRC1 PcG proteins.

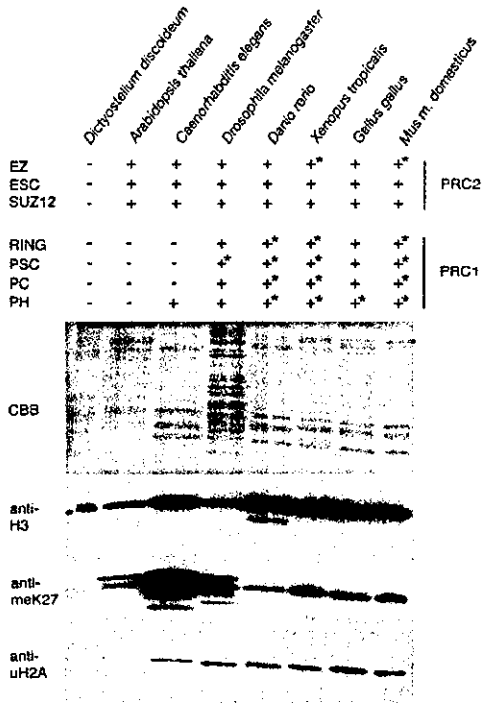

Figure 7. Evolution of H2A Ubiquitylation and PcG Proteins

Illustrated are summarized results of blast searches for homologs of the core PRC1 and PRC2 proteins, designated according to nomenclature of *D. melanogaster* proteins. Blast searches were carried out using protein sequences of both *M. m. domesticus* and *D. melanogaster* proteins. Homologs were identified based on similarity over much of the protein. Thus, proteins that showed homology only in the Ring finger, SET, or chromodomain were not considered as true PcG homologs. Species where clear homologs could be identified are indicated (+). Asterisks indicate that more than one direct homolog exists in that species. Shown below are acid-extracted histones purified from the different species (CBB) and the Western blot analysis using antibodies to histone H3 (H3), triMeH3K27 (meK27), and uH2A.

We were interested in examining other organisms to determine to what extent the occurrence of PRC1 proteins correlates with the presence of uH2A (Figure 7). We focused on organisms for which relatively complete genome sequence is available to allow us to identify putative homologs of the *Drosophila melanogaster* PRC1 (PC, PH, PSC, and dRING) and PRC2 (EZ, ESC, and SUZ12) core proteins.

We went on to determine the presence of uH2A and tri-meH3-K27 by Western blot analysis of acid-extracted histones. Detection of histone H3 provided a positive control. No homologs of either PRC1 or PRC2 proteins could be identified in the genome of the slime mold *Dictyostelium discoideum*. Consistent with this, neither H3-K27 trimethylation nor H2A ubiquitylation could be detected by Western blot analysis. *Arabidopsis thaliana* has homologs of the PRC2 proteins EZ, ESC, and SUZ12 and is also known to have H3-K27 trimethylation. There are, however, no PRC1 homologs present. Again, consistent with predictions, we detected H3-K27 trimethylation but no uH2A. Analysis of *Caenorhabditis elegans*

revealed an unexpected result. PRC2 homologs and H3-K27 trimethylation are known to be present in this organism, and indeed we detected extremely high levels of trimeH3-K27 by Western blot. However, we also detected significant levels of uH2A, despite the absence of dRING, PSC, and PC homologs.

Analysis of organisms representing a number of other kingdoms, i.e., insects (*Drosophila melanogaster*), fish (*Danio rerio*), amphibia (*Xenopus tropicalis*), birds (*Gallus gallus*), and mammals (*Mus m. domesticus*), revealed in all cases the presence of both PRC1 and PRC2 homologs. In all of these organisms, we detected significant levels both of H3-K27 trimethylation and H2A ubiquitylation. Overall, these results demonstrate that uH2A is present in organisms with dRING, PSC, and PC homologs. However, in *C. elegans* at least, other factors may be involved in H2A ubiquitylation.

Discussion

In this study, we have shown that a subset of PRC1 PcG proteins, including the Ring finger proteins Ring1B and Mel18, are recruited to the inactive X chromosome in early development. Coincident with this, we observe chromosome-wide ubiquitylation of histone H2A, suggesting a direct link between these events. In support of this, we show that deletion of Ring1B alone is sufficient to deplete global levels of uH2A in ES cells, while depletion of uH2A on Xi requires deletion of Ring1B and its closely related homolog Ring1A. Our results demonstrate a role for Ring1A/B and PcG complexes in genome-wide H2A ubiquitylation and implicate this histone modification in the maintenance of gene silencing.

H2A Ubiquitylation in X Inactivation

The close correlation of PRC1 enrichment on Xi and the appearance of uH2A, both in normal development and in differentiating ES cells, provided evidence that these events are linked. This was confirmed in analysis of cells lacking both Ring1B and Ring1A proteins. Some questions, however, remain. First, given that PRC1 enrichment is transient in early development, how is it that uH2A on Xi is maintained in more differentiated cells? Two considerations could be important for this. Detection of PRC1 protein enrichment on Xi by immunofluorescence is a relative measurement, and absence of enrichment does not equate to absence of localization. Clearly, the affinity and avidity of different antibodies will influence the probability of detecting specific nuclear localization patterns. Interchangeability of different PRC1 homologs in Xi-associated complexes also could mask localization of individual components. Thus, although in previous studies we did not detect Xi enrichment of Bmi1 (Mak et al., 2002; Silva et al., 2003), which like Mel18 is a direct homolog of *D. melanogaster* PSC, we cannot rule out that this protein is present at a lower level in Xi PRC1 complexes. Evidence for interchangeability is provided by the example of Mph2, which is enriched on Xi in TS cells, and Mph1, which is enriched on Xi in differentiating ES cells but not in TS cells.

A further point that needs to be factored is that different PRC1 homologs often show very different expression patterns through development and in different cell types. This is well illustrated by the example of Ring1A and Ring1B proteins. Ring1B is most highly expressed in early development, and deletion of the locus results in early embryo lethality (Voncken et al., 2003; M.V. and H.K., unpublished). Consistent with this, we found that Ring1B-deficient ES cells show extensive depletion of global uH2A levels. Ring1A, in contrast, is more highly expressed in differentiated cell types, and homozygous null animals are viable (Schoorlemmer et al., 1997; del Mar et al., 2000). This, in turn, is consistent with our observation that uH2A on Xi is maintained in differentiated cells by the combined action of Ring1A and Ring1B proteins.

With these facts in mind, it is reasonable to suppose that lower levels of PRC1 complexes or a multiplicity of distinct but functionally equivalent complexes are involved in maintaining uH2A on Xi beyond the time when Ring1B, Mel18, and Mph1/2 protein enrichment is readily detectable. Indeed, a similar situation occurs with the PRC2 complex, where loss of detectable enrichment on Xi in more differentiated cell types is not accompanied by loss of H3-K27 trimethylation (Silva et al., 2003; Plath et al., 2003).

A second open question is the function of H2A ubiquitylation on Xi. We analyzed expression of X-linked genes in Ring1A/B double knockout cells and did not observe evidence for X chromosome reactivation (data not shown). This may in part be because cell selection precluded examining long-term effects of uH2A depletion. It is also possible that other epigenetic modifications, for example DNA methylation, successfully maintain gene silencing in the absence of uH2A. Further studies should address the consequence of uH2A depletion on Xi in the absence of other epigenetic marks, for example trimeH3-K27.

The Role of H3-K27 Methylation in H2A Ubiquitylation

Recent studies support a model that PRC1 recruitment is facilitated by binding of the PC chromodomain to trimeH3-K27 (Cao et al., 2002; Kuzmichev et al., 2002; Fischle et al., 2003; Min et al., 2003), and clearly this provides an attractive model to explain PRC1 recruitment and H2A ubiquitylation on Xi. However, some evidence argues against this idea. First, we have been unable to detect Xi enrichment of two of the three mammalian PC homologs, Mpc2 and M33 (Mak et al., 2002; Silva et al., 2003; data not shown). While this does not rule out involvement of a different PC homolog or other chromodomain protein, a direct interaction of PRC1 proteins with *Xist* RNA should also be considered. Interestingly, a recent study has identified an RNA binding FCS finger domain in the mouse PRC1 protein Mph1, and a similar domain identified in the *C. elegans* Polycomb protein SOP-2 was shown to be required for correct localization to nuclear bodies (Zhang et al., 2004).

A second observation that challenges the model linking H3-K27 trimethylation to PRC1 recruitment is that global levels of uH2A were seen to be not directly proportional to trimethylated H3-K27 in ES cells and differentiated derivatives. We conclude that while tri-meH3-K27 may contribute to PRC1 recruitment and resultant H2A ubiquitylation, it is not the sole determinant. This

is consistent with previous work indicating that PRC1 and PRC2 complexes are recruited to distinct as well as shared target loci (Carrington and Jones, 1996; Lessard et al., 1999).

Implications for PRC1 PcG Protein Function

Our observations provide compelling evidence that Ring1A/B PcG proteins play a central role in genome-wide ubiquitylation of histone H2A, most likely functioning as H2A-specific E3 ligases. Indeed, while this manuscript was under revision, Wang et al. (2004) reported that the Ring1B protein is an E3 ligase with specificity for histone H2A lysine 119. This then raises the question of whether or not H2A ubiquitylation is required for the function of the PRC1 PcG complex in maintaining gene silencing. Ring1A/B proteins were initially identified based on two-hybrid interaction with HPC2/M33 (Satijn et al., 1997; Schoorlemmer et al., 1997) and Bmi1/Mel18 (Satijn and Otte, 1999; Suzuki et al., 2002) and therefore were not formally classified as PcG proteins. However, two recent studies have demonstrated mutations in the *D. melanogastor* homolog of Ring1A/B, dRING, in the classical Polycomb mutation *sex combs extra* (*sce*) (Fritsch et al., 2003; Gorfinkiel et al., 2004). The *sce* mutation was shown to derepress transcription of the Ubx gene, confirming the designation of dRING as a classical PcG protein. Moreover, Ubx derepression was also observed in a hypomorphic *sce* allele with a point mutation affecting a single residue in the Ring finger domain of the dRING protein (Fritsch et al., 2003). These observations, together with the role of Ring1B in H2A ubiquitylation, suggest that this histone modification is important for gene repression by PRC1 PcG protein complexes.

A large body of evidence demonstrates that PRC1 can interfere both with chromatin remodeling and transcription through an energy-independent interaction with chromatin templates (Shao et al., 1999; Francis et al., 2001; Levine et al., 2002; King et al., 2002). How can these observations be reconciled with our data implicating H2A ubiquitylation as a mechanism of PRC1 function? A possible explanation is that PRC1 and remodeling/transcription complexes compete for core nucleosomal surfaces in vitro and that this occurs independent of H2A ubiquitylation. This mechanism was indeed proposed by Francis et al. (2001) to account for the fact that chromatin templates must be pretreated with PRC1 complexes in order to inhibit SWI-SNF activity in vitro.

Assuming that H2A ubiquitylation is important for PRC1 function in the maintenance of gene repression, how might this occur? Both direct and indirect mechanisms can be envisaged. The large size of the ubiquitin group compared to other histone modifications would be consistent with it interfering directly with nucleosome dynamics during transcription. Perhaps relevant to this is evidence indicating that H2A/H2B dimers are displaced from nucleosomes during transcription by RNA polymerase II (Kireeva et al., 2002; Belotserkovskaya et al., 2003). Such a model would also be consistent with recent experiments demonstrating that PcG complexes interfere with initiation of transcription but not with recruitment of TBP and RNA polymerase II (Dellino et al., 2004). An indirect model, postulating recruitment of effector proteins to monoubiquitylated H2A, is also compatible with the aforementioned observations. Alternatively, uH2A may function through a transhistone regulatory pathway, as has been reported for H2B ubiquitylation in *S. cerevisiae* (Sun and Allis, 2002; Dover et al., 2002; Briggs et al., 2002). Loss of uH2A in Ring1B$^{-/-}$ ES cells had no obvious impact on H3-K27 methylation levels (Figure 4E), but other modifications have not yet been analyzed.

Experimental Procedures

Mouse Strains, Embryos, and Cell Lines

Preimplantation and postimplantation mouse embryos were isolated from timed matings of (C57Bl6 × CBA)F1 animals as described previously (Sheardown et al., 1997; Silva et al., 2003). Derivation and maintenance of XX ES cells (PGK12.1), XX TS cells (B7), and XY TS cells (B1) is described in detail by Penny et al. (1996) and Mak et al. (2002). Adult and embryonic XX fibroblast cells and cell lines were derived as described previously (Duthie et al., 1999; Silva et al., 2003). XY ES cell lines 8A and 12E carry inducible *Xist* transgenes integrated into random autosomal sites. They were established essentially as described by Wutz and Jaenisch (2000), except that the pTRE-tight vector (Clontech) was used to clone full-length *Xist* cDNA (further details available on request). Transgenic *Xist* RNA was undetectable in uninduced cells. *Xist* expression was induced by culturing in the presence of 1 μg/ml doxycycline.

Ring1A-deficient mice were as described previously (del Mar et al., 2000). Full details of conditional gene targeting of Ring1B and analysis of Ring1B$^{-/-}$ embryos will be provided in a subsequent manuscript (M.V. and H.K., unpublished). The 10-3 and 13-3 ES cell lines were derived from blastocysts from crosses between homozygous Ring1B$^{fl/fl}$ animals. Conditional deletion of Ring1B was carried out by transient transfection with the pCRE-Pac plasmid expressing CRE recombinase, as described by Taniguchi et al. (1998). Cell lines were tested for the presence of a Y chromosome by PCR analysis of the Y-linked Sry gene. Complementation analysis was carried out using a Ring1B cDNA construct with an N-terminal myc Tag cloned into the chicken β-actin promoter construct pCXN2 (Niwa et al., 1991). 10-3 Ring1B$^{-/-}$ ES cells were transfected using Lipofectamin 2000 following standard protocols. Pooled stable transfectants were expanded under G418 selection prior to extraction of proteins for Western blot analysis.

CRE-mediated deletion of Ring1B in MEF cell lines using AdCre virus was carried out as described previously (Kanegae et al., 1995).

Antibodies

For immunofluorescence (IF) and Westerns (W), the following antibodies and dilutions were used: rabbit polyclonal antibodies to Su(z)12 from Upstate (1:200 in IF); rabbit polyclonal Mel18 (H-115) from Santa Cruz Biotechnology (1:50 in IF); mouse monoclonal antibody clone FK2 from Affiniti research products, which recognizes ubiquitylated proteins (1:300 in IF and 1:1000 in W); mouse monoclonal antibody clone FK1 from Affiniti research products, which recognizes polyubiquitylated proteins (1:50 in IF); mouse monoclonal IgM anti-ubiquitylated-histone H2A (clone E6C5) from Upstate (1:50 in IF and 1:400 in W); and rabbit polyclonal antibody to Histone H3-ChIP grade (ab1791) abcam (1:10,000 in W). Antibodies to Eed, Ezh2, HPH1, Mph1, Ring1A, Ring1B, and tri-meH3-K27 (6523) have been previously described (Sewalt et al., 1998; Satijn et al., 1997; Atsuta et al., 2001; Peters et al., 2003). Mouse monoclonal antibody to Mph2 will be described in detail in a subsequent communication (H.K., unpublished).

Immunofluorescence and RNA FISH

For immunofluorescence, TS cells, fibroblasts, and cells from trypsin-dissociated postimplantation embryos were placed on slides in medium and left to attach for 2–4 hr. Generally for Eed, Ezh2, Su(z)12, Ring1B, Mel18, Mph1, Mph2, and tri-meH3K27 antibodies, cells were rinsed in PBS, fixed in 2% paraformaldehyde (PFA) for 15 min at room temperature, rinsed in PBS, and permeabilized for 5 min in

0.4% Triton X. For FK2, FK1, and uH2A antibodies, or double labeling experiments including any of these, cells were first permeabilized and then fixed. In ES cell differentiation experiments, cells were resuspended in PBS at a concentration of 1×10^6 cells/ml. For FK2, FK1, uH2A, and tri-meH3-K27 antibodies, cells were cytospun onto slides in PBS (100 μl/slide, 8 min, 1800 rpm). Slides were rinsed in PBS, permeabilized, and fixed. When using Eed, Su(z)12, Ring1B, Mel18, and Mph1 antibodies, cells were resuspended to the same concentration in 2% PFA, fixed for 15 min at room temperature, cytospun onto slides in 2% PFA (100 μl/slide, 8 min, 1800 rpm), rinsed in PBS, and permeabilized. Immunofluorescence was carried out as described by Mak et al. (2002). Procedures for immunofluorescence on preimplantation embryos have been described previously (Silva et al., 2003). For cytospun cells, *Xist* RNA FISH was essentially carried out as described in Duthie et al. (1999), except that after 25 min fixation on ice, cells were cytospun in fixation solution. For cells plated on slides, RNA FISH was carried out as described in Silva et al. (2003). Images were acquired on a Leica DMRB microscope equipped with a CCD camera or on a Leica SP1 confocal microscope.

Extracts and Western Blot Analysis

Histone extractions from mouse tissue culture cells were performed as follows. Trypsinized cells were washed in PBS and pellets were flash-frozen. When preparing histones from ES cells, in order to minimize feeder contamination, cells were plated repeatedly for periods of 10–30 min on nongelatinized plates. Frozen cell pellets of approximately 100 μl were rapidly thawed, washed in ice-cold PBS containing protease inhibitors, spun down (4 min, 235 × g, 4°C), resuspended in ice-cold PBS containing protease inhibitors, and incubated on ice for 10 min. After centrifugation, pellets were resuspended in 1 ml of ice cold 0.2 M H_2SO_4 and incubated on ice for 30 min. Samples were then spun down (2 min, 20,200 × g, 4°C). The supernatant was precipitated by adding TCA to a final concentration of 25% and leaving on ice for 30 min. Precipitated histones were pelleted (10 min, 20,200 × g, 4°C) and washed twice by adding 1 ml of ice cold acetone and incubating 10 min on ice. After centrifugation (10 min, 20,200 × g, 4°C), pellets were dissolved in 100 mM Tris (pH 7.6).

Histone extractions from *A. thaliana*, *C. elegans*, *X. tropicalis* (liver), *D. rerio*, *D. melanogastor* Schneider 2 cells, and *G. gallus* DT140 cells were processed as described by Jackson et al. (2004). Specifically, material was ground with a mortar and pestle under liquid nitrogen and resuspended in NIB buffer (15 mM PIPES [pH 6.8], 5 mM $MgCl_2$, 60 mM KCL, 0.25 sucrose, 15 mM NaCl, 1 mM $CaCl_2$, 0.8% Triton X100 containing protease inhibitors). For ground material comprising about 400 μl powder, 5 ml of buffer were used and filtered through muslin cloth. Samples were centrifuged at 10,000 × g for 20 min. The pellet (nuclei) was subsequently extracted twice with 0.4 M H_2SO_4. Supernatants were precipitated with 10–12 volumes of precooled acetone for 1 hr at −20°C and spun at 20,200 × g for 5 min at 4°C. Pellets were dissolved in 100 mM Tris (pH 7.6). Whole-cell and nuclear extracts were prepared as described previously (Mermoud et al., 1999).

For Western blotting, 5 μg of the histone extracts were loaded per lane and electrophoresed by SDS-PAGE using 8%–16% gradient gels. Westerns were performed following the protocols provided by each antibody supplier. Secondary antibodies were polyclonal goat anti-mouse immunoglobulins/HRP (DakoCytomation), sheep anti-mouse IgG HPR linked (Amersham), and donkey anti-rabbit Ig HPR linked (Amersham). ECL detection (Amersham) was carried out according to manufacturer's recommendations.

Acknowledgments

We would like to thank Catherine Pears and Louis Mahadevan for histone preparations from *Dictyostelium Discoideum*; Vincent Colot, Justin Goodrich, Peter Shaw, Bill Earnshaw, Mario de Bono, James Briscoe, Lyle Zimmerman, and Fillipa Carreira-Barbosa for materials and help with histone preparation from various species; Izumo Saito and Masakatsu Yamashita for Ad-Cre virus; Thomas Jenuwein for antibodies; and other lab members for critical reading of the manuscript. This work was supported by the Medical Research Council, UK, by Special Coordination Funds for Promoting Science and Technology from the Japanese Government, and by the DGI, Spanish Ministry of Education and Science (SAF2001-2211-CO2-01). M.d.N. is supported by Programa Gulbenkian de Doutoramento em Biologia e Medicina, Portugal.

Received: August 19, 2004
Revised: October 14, 2004
Accepted: October 15, 2004
Published online: November 1, 2004

References

Atsuta, T., Fujimura, S., Moriya, H., Vidal, M., Akasaka, T., and Koseki, H. (2001). Production of monoclonal antibodies against mammalian Ring1B protein. Hybridoma *20*, 43–46.

Baarends, W.M., Hoogerbrugge, J.W., Roest, H.P., Ooms, M., Vreeburg, J., Hoeijmakers, J.H., and Grootegoed, J.A. (1999). Histone ubiquitylation and chromatin remodeling in mouse spermatogenesis. Dev. Biol. *207*, 322–333.

Bannister, A.J., Zegerman, P., Partridge, J.F., Miska, E.A., Thomas, J.O., Allshire, R.C., and Kouzarides, T. (2001). Selective recognition of methylated lysine 9 on histone H3 by the HP1 chromo domain. Nature *410*, 120–124.

Belotserkovskaya, R., Oh, S., Bondarenko, V.A., Orphanides, G., Studitsky, V.M., and Reinberg, D. (2003). FACT facilitates transcription-dependent nucleosome alteration. Science *301*, 1090–1093.

Briggs, S.D., Xiao, T., Sun, Z.W., Caldwell, J.A., Shabanowitz, J., Hunt, D.F., Allis, C.D., and Strahl, B.D. (2002). Gene silencing: trans-histone regulatory pathway in chromatin. Nature *418*, 498.

Brockdorff, N., Ashworth, A., Kay, G.F., McCabe, V.M., Norris, D.P., Cooper, P.J., Swift, S., and Rastan, S. (1992). The product of the mouse *Xist* gene is a 15 kb inactive X-specific transcript containing no conserved ORF and located in the nucleus. Cell *71*, 515–526.

Brown, C.J., Ballabio, A., Rupert, J.L., Lafreniere, R.G., Grompe, M., Tonlorenzi, R., and Willard, H.F. (1991). A gene from the region of the human X inactivation centre is expressed exclusively from the inactive X chromosome. Nature *349*, 38–44.

Brown, C.J., Hendrich, B.D., Rupert, J.L., Lafreniere, R.G., Xing, Y., Lawrence, J., and Willard, H.F. (1992). The human *XIST* gene: analysis of a 17 kb inactive X-specific RNA that contains conserved repeats and is highly localized within the nucleus. Cell *71*, 527–542.

Cao, R., Wang, L., Wang, H., Xia, L., Erdjument-Bromage, H., Tempst, P., Jones, R.S., and Zhang, Y. (2002). Role of histone H3 lysine 27 methylation in Polycomb-group silencing. Science *298*, 1039–1043.

Carrington, E.A., and Jones, R.S. (1996). The *Drosophila* Enhancer of Zeste gene encodes a chromosomal protein: examination of wild-type and mutant protein distribution. Development *122*, 44073–44083.

Czermin, B., Melfi, R., McCabe, D., Seitz, V., Imhof, A., and Pirrotta, V. (2002). *Drosophila* enhancer of Zeste/ESC complexes have a histone H3 methyltransferase activity that marks chromosomal Polycomb sites. Cell *111*, 185–196.

Dawson, B.A., Herman, T., Haas, A.L., and Lough, J. (1991). Affinity isolation of active murine erythroleukemia cell chromatin: uniform distribution of ubiquitylated histone H2A between active and inactive fractions. J. Cell. Biochem. *46*, 166–173.

del Mar, L.M., Marcos-Gutierrez, C., Perez, C., Schoorlemmer, J., Ramirez, A., Magin, T., and Vidal, M. (2000). Loss- and gain-of-function mutations show a polycomb group function for Ring1A in mice. Development *127*, 5093–5100.

Dellino, G.I., Schwartz, Y.B., Farkas, G., McCabe, D., Elgin, S.C., and Pirrotta, V. (2004). Polycomb silencing blocks transcription initiation. Mol. Cell *13*, 887–893.

Dover, J., Schneider, J., Tawiah-Boateng, M.A., Wood, A., Dean, K., Johnston, M., and Shilatifard, A. (2002). Methylation of histone H3 by COMPASS requires ubiquitylation of histone H2B by Rad6. J. Biol. Chem. *277*, 28368–28371.

Duthie, S.M., Nesterova, T.B., Formstone, E.J., Keohane, A.M.,

Turner, B.M., Zakian, S.M., and Brockdorff, N. (1999). *Xist* RNA exhibits a banded localization on the inactive X chromosome and is excluded from autosomal material in cis. Hum. Mol. Genet. *8*, 195–204.

Erhardt, S., Su, I.H., Schneider, R., Barton, S., Bannister, A.J., Perez-Burgos, L., Jenuwein, T., Kouzarides, T., Tarakhovsky, A., and Surani, M.A. (2003). Consequences of the depletion of zygotic and embryonic enhancer of zeste 2 during preimplantation mouse development. Development *130*, 4235–4248.

Fischle, W., Wang, Y.M., Jacobs, S.A., Kim, Y.C., Allis, C.D., and Khorasanizadeh, S. (2003). Molecular basis for the discrimination of repressive methyl-lysine marks in histone H3 by Polycomb and HP1 chromodomains. Genes Dev. *17*, 1870–1881.

Francis, N.J., Saurin, A.J., Shao, Z., and Kingston, R.E. (2001). Reconstitution of a functional core polycomb repressive complex. Mol. Cell *8*, 545–556.

Fritsch, C., Beuchle, D., and Muller, J. (2003). Molecular and genetic analysis of the Polycomb group gene Sex combs extra/Ring in *Drosophila*. Mech. Dev. *120*, 949–954.

Fujimuro, M., Sawada, H., and Yokosawa, H. (1994). Production and characterization of monoclonal antibodies specific to multi-ubiquitin chains of polyubiquitylated proteins. FEBS Lett. *349*, 173–180.

Goldknopf, I.L., Taylor, C.W., Baum, R.M., Yeoman, L.C., Olson, M.O., Prestayko, A.W., and Busch, H. (1975). Isolation and characterization of protein A24, a "histone-like" non-histone chromosomal protein. J. Biol. Chem. *250*, 7182–7187.

Gorfinkiel, N., Fanti, L., Melgar, T., Garcia, E., Pimpinelli, S., Guerrero, I., and Vidal, M. (2004). The *Drosophila* Polycomb group gene Sex combs extra encodes the ortholog of mammalian Ring1 proteins. Mech. Dev. *121*, 449–462.

Heard, E. (2004). Recent advances in X-chromosome inactivation. Curr. Opin. Cell Biol. *16*, 247–255.

Huang, S.Y., Bernard, M.B., Xu, M., Matsui, S., Rose, S.M., and Garrard, W.T. (1986). The active immunoglobulin kappa chain gene is packaged by non-ubiquitin-conjugated nucleosomes. Proc. Natl. Acad. Sci. USA *83*, 3738–3742.

Jackson, J.P., Johnson, L., Jasencakova, Z., Zhang, X., Perez-Burgos, L., Singh, P.B., Cheng, X., Schubert, I., Jenuwein, T., and Jacobsen, S.E. (2004). Dimethylation of histone H3 lysine 9 is a critical mark for DNA methylation and gene silencing in *Arabidopsis thaliana*. Chromosoma *112*, 308–315.

Jenuwein, T., and Allis, C.D. (2001). Translating the histone code. Science *293*, 1074–1080.

Kanegae, Y., Lee, G., Sato, Y., Tanaka, M., Nakai, M., Sakaki, T., Sugano, S., and Saito, I. (1995). Efficient gene activation in mammalian cells by using recombinant adenovirus expressing site-specific Cre recombinase. Nucleic Acids Res. *23*, 3816–3821.

King, I.F., Francis, N.J., and Kingston, R.E. (2002). Native and recombinant polycomb group complexes establish a selective block to template accessibility to repress transcription in vitro. Mol. Cell. Biol. *22*, 7919–7928.

Kireeva, M.L., Walter, W., Tchernajenko, V., Bondarenko, V., Kashlev, M., and Studitsky, V.M. (2002). Nucleosome remodeling induced by RNA polymerase II: loss of the H2A/H2B dimer during transcription. Mol. Cell *9*, 541–552.

Kohlmaier, A., Savarese, F., Lachner, M., Martens, J., Jenuwein, T., and Wutz, A. (2004). A chromosomal memory triggered by *Xist* regulates histone methylation in X inactivation. PLoS. Biol. 2(7), E171.

Kuzmichev, A., Nishioka, K., Erdjument-Bromage, H., Tempst, P., and Reinberg, D. (2002). Histone methyltransferase activity associated with a human multiprotein complex containing the Enhancer of Zeste protein. Genes Dev. *16*, 2893–2905.

Lachner, M., O'Carroll, D., Rea, S., Mechtler, K., and Jenuwein, T. (2001). Methylation of histone H3 lysine 9 creates a binding site for HP1 proteins. Nature *410*, 116–120.

Lessard, J., Schumacher, A., Thorsteinsdottir, U., van Lohuizen, M., Magnuson, T., and Sauvageau, G. (1999). Functional antagonism of the Polycomb-Group genes eed and Bmi1 in hemopoietic cell proliferation. Genes Dev. *13*, 2691–2703.

Levine, S.S., Weiss, A., Erdjument-Bromage, H., Shao, Z., Tempst, P., and Kingston, R.E. (2002). The core of the polycomb repressive complex is compositionally and functionally conserved in flies and humans. Mol. Cell. Biol. *22*, 6070–6078.

Levinger, L., and Varshavsky, A. (1982). Selective arrangement of ubiquitylated and D1 protein-containing nucleosomes within the *Drosophila* genome. Cell *28*, 375–385.

Mak, W., Baxter, J., Silva, J., Newall, A.E., Otte, A.P., and Brockdorff, N. (2002). Mitotically stable association of polycomb group proteins eed and enx1 with the inactive x chromosome in trophoblast stem cells. Curr. Biol. *12*, 1016–1020.

Mak, W., Nesterova, T.B., de Napoles, M., Appanah, R., Yamanaka, S., Otte, A.P., and Brockdorff, N. (2004). Reactivation of the paternal X chromosome in early mouse embryos. Science *303*, 666–669.

Mermoud, J.E., Costanzi, C., Pehrson, J.R., and Brockdorff, N. (1999). Histone macroH2A1.2 relocates to the inactive X chromosome after initiation and propagation of X-inactivation. J. Cell Biol. *147*, 1399–1408.

Min, J.R., Zhang, Y., and Xu, R.M. (2003). Structural basis for specific binding of polycomb chromodomain to histone H3 methylated at Lys 27. Genes Dev. *17*, 1823–1828.

Muller, J., Hart, C.M., Francis, N.J., Vargas, M.L., Sengupta, A., Wild, B., Miller, E.L., O'Connor, M.B., Kingston, R.E., and Simon, J.A. (2002). Histone methyltransferase activity of a *Drosophila* Polycomb group repressor complex. Cell *111*, 197–208.

Nickel, B.E., and Davie, J.R. (1989). Structure of polyubiquitylated histone H2A. Biochemistry *28*, 964–968.

Nickel, B.E., Allis, C.D., and Davie, J.R. (1989). Ubiquitylated histone H2B is preferentially located in transcriptionally active chromatin. Biochemistry *28*, 958–963.

Niwa, H., Yamamura, K., and Miyazaki, J. (1991). Efficient selection for high-expression transfectants with a novel eukaryotic vector. Gene *108*, 193–199.

Okamoto, I., Otte, A.P., Allis, C.D., Reinberg, D., and Heard, E. (2004). Epigenetic dynamics of imprinted X inactivation during early mouse development. Science *303*, 644–649.

Parlow, M.H., Haas, A.L., and Lough, J. (1990). Enrichment of ubiquitylated histone H2A in a low salt extract of micrococcal nuclease-digested myotube nuclei. J. Biol. Chem. *265*, 7507–7512.

Penny, G.D., Kay, G.F., Sheardown, S.A., Rastan, S., and Brockdorff, N. (1996). Requirement for *Xist* in X chromosome inactivation. Nature *379*, 131–137.

Peters, A.H.F.M., Kubicek, S., Mechtler, K., O'Sullivan, R.J., Derijck, A.A.H.A., Perez-Burgos, L., Kohlmaier, A., Opravil, S., Tachibana, M., Shinkai, Y., et al. (2003). Partitioning and plasticity of repressive histone methylation states in mammalian chromatin. Mol. Cell *12*, 1577–1589.

Pickart, C.M. (2001). Mechanisms underlying ubiquitination. Annu. Rev. Biochem. *70*, 503–533.

Plath, K., Fang, J., Mlynarczyk-Evans, S.K., Cao, R., Worringer, K.A., Wang, H.B., de la Cruz, C.C., Otte, A.P., Panning, B., and Zhang, Y. (2003). Role of histone H3 lysine 27 methylation in X inactivation. Science *300*, 131–135.

Robzyk, K., Recht, J., and Osley, M.A. (2000). Rad6-dependent ubiquitylation of histone H2B in yeast. Science *287*, 501–504.

Satijn, D.P., Gunster, M.J., van der Vlag, V., Hamer, K.M., Schul, W., Alkema, M.J., Saurin, A.J., Freemont, P.S., van Driel, R., and Otte, A.P. (1997). RING1 is associated with the polycomb group protein complex and acts as a transcriptional repressor. Mol. Cell. Biol. *17*, 4105–4113.

Satijn, D.P., and Otte, A.P. (1999). RING1 interacts with multiple Polycomb-group proteins and displays tumorigenic activity. Mol. Cell. Biol. *19*, 57–68.

Schoorlemmer, J., Marcos-Gutierrez, C., Were, F., Martinez, R., Garcia, E., Satijn, D.P., Otte, A.P., and Vidal, M. (1997). Ring1A is a

transcriptional repressor that interacts with the Polycomb-M33 protein and is expressed at rhombomere boundaries in the mouse hindbrain. EMBO J. *16*, 5930–5942.

Sewalt, R.G., van der Vlag, V., Gunster, M.J., Hamer, K.M., den Blaauwen, J.L., Satijn, D.P., Hendrix, T., van Driel, R., and Otte, A.P. (1998). Characterization of interactions between the mammalian polycomb-group proteins Enx1/EZH2 and EED suggests the existence of different mammalian polycomb-group protein complexes. Mol. Cell. Biol. *18*, 3586–3595.

Shao, Z.H., Raible, F., Mollaaghababa, R., Guyon, J.R., Wu, C.T., Bender, W., and Kingston, R.E. (1999). Stabilization of chromatin structure by PRC1, a polycomb complex. Cell *98*, 37–46.

Sheardown, S.A., Duthie, S.M., Johnston, C.M., Newall, A.E., Formstone, E.J., Arkell, R.M., Nesterova, T.B., Alghisi, G.C., Rastan, S., and Brockdorff, N. (1997). Stabilization of *Xist* RNA mediates initiation of X chromosome inactivation. Cell *91*, 99–107.

Silva, J., Mak, W., Zvetkova, I., Appanah, R., Nesterova, T.B., Webster, Z., Peters, A.H.F.M., Jenuwein, T., Otte, A.P., and Brockdorff, N. (2003). Establishment of histone H3 methylation on the inactive X chromosome requires transient recruitment of Eed-Enx1 Polycomb group complexes. Dev. Cell *4*, 481–495.

Strahl, B.D., and Allis, C.D. (2000). The language of covalent histone modifications. Nature *403*, 41–45.

Sun, Z.W., and Allis, C.D. (2002). Ubiquitylation of histone H2B regulates H3 methylation and gene silencing in yeast. Nature *418*, 104–108.

Suzuki, M., Mizutani-Koseki, Y., Fujimura, Y., Miyagishima, H., Kaneko, T., Takada, Y., Akasaka, T., Tanzawa, H., Takihara, Y., Nakano, M., et al. (2002). Involvement of the Polycomb-group gene Ring1B in the specification of the anterior-posterior axis in mice. Development *129*, 4171–4183.

Taniguchi, M., Sanbo, M., Watanabe, S., Naruse, I., Minshina, M., and Yagi, T. (1998). Efficient production of Cre-mediated site directed recombinants through the utilization of the puromycin resistance gene, pac; a transient gene-integration marker for ES cells. Nucleic Acids Res. *26*, 679–680.

Turner, B.M. (2002). Cellular memory and the histone code. Cell *111*, 285–291.

Vassilev, A.P., Rasmussen, H.H., Christensen, E.I., Nielsen, S., and Celis, J.E. (1995). The levels of ubiquitylated histone H2A are highly upregulated in transformed human cells: partial colocalization of uH2A clusters and PCNA/cyclin foci in a fraction of cells in S-phase. J. Cell Sci. *108*, 1205–1215.

Voncken, J.W., Roelen, B.A., Roefs, M., de Vries, S., Verhoeven, E., Marino, S., Deschamps, J., and van Lohuizen, M. (2003). Rnf2 (Ring1b) deficiency causes gastrulation arrest and cell cycle inhibition. Proc. Natl. Acad. Sci. USA *100*, 2468–2473.

Wang, J., Mager, J., Chen, Y., Schneider, E., Cross, J.C., Nagy, A., and Magnuson, T. (2001). Imprinted X inactivation maintained by a mouse Polycomb group gene. Nat. Genet. *28*, 371–375.

Wang, H., Wang, L., Erdjument-Bromage, H., Vidal, M., Tempst, P., Jones, R.S., and Zhang, Y. (2004). Role of histone H2A ubiquitination in Polycomb silencing. Nature *431*, 873–878.

Wutz, A., and Jaenisch, R. (2000). A shift from reversible to irreversible X inactivation is triggered during ES cell differentiation. Mol. Cell *5*, 695–705.

Zhang, Y. (2003). Transcriptional regulation by histone ubiquitination and deubiquitination. Genes Dev. *17*, 2733–2740.

Zhang, H., Christoforou, A., Aravind, L., Emmons, S.W., van den Heuvel, S., and Haber, D.A. (2004). The *C. elegans* Polycomb gene sop-2 encodes an RNA binding protein. Mol. Cell *14*, 841–847.